ANNUAL REVIEWS

Annual Review of Fluid Mechanics

Nonideal Compressible Fluid Dynamics of Dense Vapors and Supercritical Fluids

Alberto Guardone,[1] Piero Colonna,[2] Matteo Pini,[2] and Andrea Spinelli[3]

[1]Department of Aerospace Science and Technology, Politecnico di Milano, Milano, Italy

[2]Propulsion and Power, Aerospace Engineering, Delft University of Technology, Delft, The Netherlands; email: p.colonna@tudelft.nl

[3]Department of Energy, Politecnico di Milano, Milano, Italy

Annu. Rev. Fluid Mech. 2024. 56:241–69

The *Annual Review of Fluid Mechanics* is online at fluid.annualreviews.org

https://doi.org/10.1146/annurev-fluid-120720-033342

Keywords

nonideal compressible fluid dynamics, nonideal thermodynamics, fundamental derivative of gas dynamics, supercritical carbon dioxide flows and power systems, organic Rankine cycle power systems, supercritical injection

Abstract

The gas dynamics of single-phase nonreacting fluids whose thermodynamic states are close to vapor-liquid saturation, close to the vapor-liquid critical point, or in supercritical conditions differs quantitatively and qualitatively from the textbook gas dynamics of dilute, ideal gases. Due to nonideal fluid thermodynamic properties, unconventional gas dynamic effects are possible, including nonclassical rarefaction shock waves and the nonmonotonic variation of the Mach number along steady isentropic expansions. This review provides a comprehensive theoretical framework of the fundamentals of nonideal compressible fluid dynamics (NICFD). The relation between nonideal gas dynamics and the complexity of the fluid molecules is clarified. The theoretical, numerical, and experimental tools currently employed to investigate NICFD flows and related applications are reviewed, followed by an overview of industrial processes involving NICFD, ranging from organic Rankine and supercritical CO_2 cycle power systems to supercritical processes. The future challenges facing researchers in the field are briefly outlined.

1. INTRODUCTION

Polytropic ideal gas: $Pv = RT$ and constant specific heats; T is the temperature, v the volume per unit mass, $R = \mathcal{R}/\mu$ with $\mathcal{R}$ the universal gas constant, and μ the molar mass

Energy equipartition principle: each fully activated degree of freedom contributes $R/2$ to the overall value of the isochoric specific heat, so that $c_v = N\mathcal{R}/(2\mu)$

Molar mass μ and molecular complexity: these are independent quantities; μ depends on the atomic species and the number of atoms; the complexity on the number of atoms and on molecular arrangement

Contrary to incompressible fluid flows, a distinctive feature of compressible flows is the influence of the fluid thermodynamic state on flow evolution. For example, the propagation velocity within the flow of small-amplitude pressure disturbances, i.e., the speed of sound c, is a thermodynamic property defined as

$$c^2 = \left(\frac{\partial P}{\partial \rho}\right)_s, \qquad 1.$$

where P is the pressure, ρ the density, and s the entropy per unit mass. In most gas dynamics studies, the thermodynamic properties of the fluid are computed using the polytropic ideal gas model.

In its simplicity, the expression of the ideal gas sound speed reveals the effect of fluid properties on the speed of sound. The gas constant R is inversely proportional to the molar mass of the substance. Hence, the speed of sound is lower for compounds made of heavier molecules. The value of specific heat c_v in the dilute gas limit is related to the number N of active degrees of freedom of a molecule according to the energy equipartition principle (Callen 1985). For a polytropic ideal gas, $\gamma = c_P/c_v = (1 + 2/N)$, with c_v and c_P the isochoric and isobaric specific heats. Hence, $c^2 = \gamma RT = (1 + 2/N)(\mathcal{R}/\mu)T$.

In this review, the number of the active degrees of freedom of a molecule N is used as a proxy for molecular complexity, with increasing values of N corresponding to more complex molecular arrangements, as discussed by Colonna & Guardone (2006).

The ideal gas region or dilute gas region features states with $Z \approx 1$ at low pressure (see **Figure 1**). Z is the compressibility factor

$$Z = \frac{Pv}{RT}, \qquad 2.$$

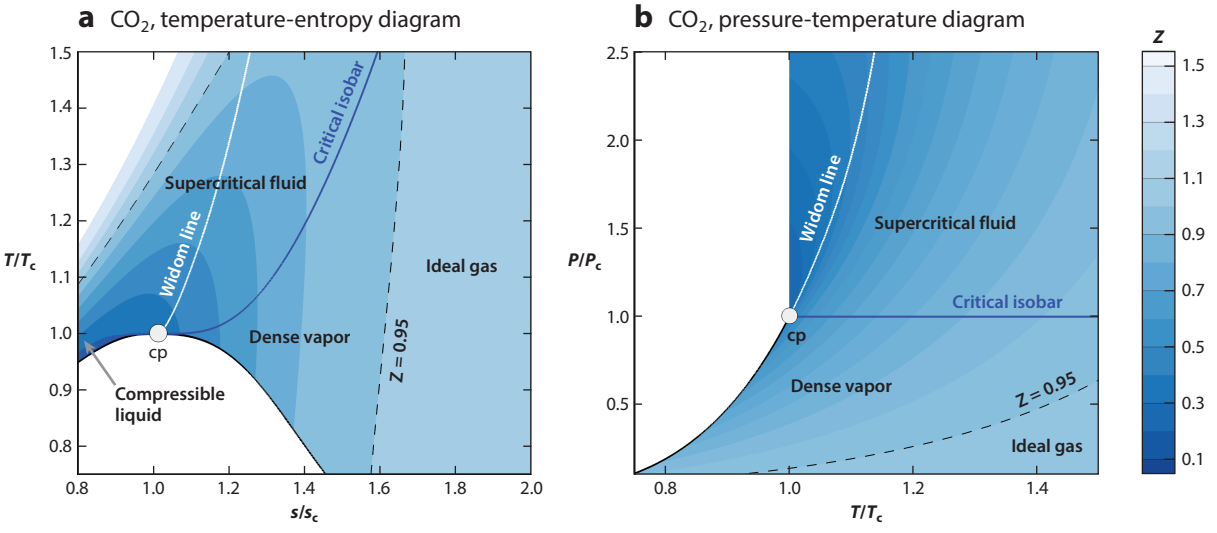

Figure 1

Exemplary fluid thermodynamic diagrams showing regions featuring varying values of the compressibility factor, Z, where P is pressure, P_c is critical pressure, s is entropy, s_c is critical entropy, T is temperature, and T_c is critical temperature. The critical point (cp) is also indicated.

and it is identical to one for a fluid in the ideal gas state. States are termed supercritical if both the pressure and temperature are greater than the vapor-liquid critical values, i.e., $P > P_c$ and $T > T_c$, or subcritical for lower values of pressure or temperature. The dense vapor region encompasses vapor states at subcritical pressure featuring $Z < 1$. The compressible liquid region identifies subcritical temperature states for which the density can change appreciably. Ideal liquid states are those for which the density does not change significantly, thus at lower temperatures. The bubble line is formed by the saturated liquid states from the triple point up to the critical point. Conversely, the dew line encompasses all the saturated vapor states from the triple point to the critical point. The critical region includes states near the vapor-liquid critical point. Several thermodynamic and transport properties diverge or go to zero in the critical point region. For example, c_v weakly diverges to infinity, c_P and the isothermal compressibility diverge to infinity, and the thermodynamic, or zero-frequency, sound speed weakly approaches zero. In the supercritical region, the Widom line (Banuti 2015) identifies states for which c_P is maximum at a given pressure. Therefore, the Widom line separates so-called liquid-like states from vapor-like states and continues the vapor-liquid equilibrium line in the P-T thermodynamic plane (**Figure 1*b***). The Widom line vanishes for $P \gtrsim 3P_c$. The square of the speed of sound, c^2, is proportional to the slope of the isentropes in the P-v plane; therefore, its value for ideal and nonideal states is different.

The departure from the ideal gas sound speed increases with the increasing complexity of the fluid molecules, thus often leading to the misconception that nonideal compressible fluid dynamic (NICFD) phenomena affect only the flows of molecularly complex fluids. On the contrary, nonideal gas dynamic phenomena influence the flows of all fluids if their thermodynamic states are in the nonideal thermodynamic region, including those of fluids made of the simplest molecules. However, nonideal effects are more pronounced for molecularly complex fluids, such as heavy hydrocarbons or fluorinated compounds used as working fluids in organic Rankine cycle (ORC) engines or refrigeration systems.

The higher the molecular complexity of the fluid, the stronger the nonideal gas dynamic effects in the flow, possibly to the point that flow phenomena are not only quantitatively different from those occurring in ideal gas flows but also qualitatively different, like, e.g., nonclassical rarefaction shock waves (Thompson & Lambrakis 1973, Menikoff & Plohr 1989, Kluwick 2001). Another example of nonideal effect is the nonmonotonic variation of the Mach number in steady isentropic expansions (Cramer & Best 1991), as opposed to the well-known monotonic increase of the Mach number from rest to supersonic conditions occurring for ideal gas flows through converging-diverging nozzles of, e.g., rocket engines.

This review concerns the gas dynamics of single-phase fluid flows if the fluid is in nonideal thermodynamic states, the states forming the nonideal single-phase thermodynamic region, assuming that the fluid is a Newtonian continuum at thermodynamic and chemical (i.e., thermochemical) equilibrium. This novel branch of fluid mechanics is termed NICFD. In the past, this type of flow was referred to as dense gas flow (or dense vapor flow), a nomenclature that refers only to dense vapor flows and does not include, e.g., flows of fluids in supercritical states. Moreover, the terminology of dense gas (or dense vapor) flows has been used in the literature as a synonym for nonclassical gas dynamic flows, which are admissible only for a subset of fluids characterized by very high molecular complexity (HMC), the so-called Bethe-Zel'dovich-Thompson (BZT) fluids. An analogous nomenclature problem arises in the case of so-called real gas flows. This terminology historically refers to chemically reacting flows of dilute gases in either chemical and thermal equilibrium or disequilibrium. Given the similarities of the governing equations and the related numerical solution methodologies (see Section 3.1), the term real gas flow is often used in the literature to refer to nonideal fluid flows, thereby possibly causing misunderstanding. For

Nonideal compressible fluid dynamics (NICFD): the gas dynamics of fluids in thermodynamic and chemical equilibrium if the thermodynamic states of the fluid is nonideal, i.e., if for the states $Z \neq 1$

Rarefaction shock waves: shock waves across which the density and the pressure decrease are physically admissible

Nonideal single-phase thermodynamic region: the nonideal thermodynamic region encompasses all single-phase thermodynamic states at thermochemical equilibrium resulting in the fluid being a dense vapor, a supercritical fluid, or a compressible liquid

these reasons, the authors discourage using the terms dense gas, dense vapor, or real gas flows if referring to the NICFD flows of interest here. More details about all topics treated here are in the **Supplemental Material**.

Supplemental Material >

Reduced state variable: a state variable is reduced if scaled by its critical point value, e.g., $T_r = T/T_c$

Principle of corresponding states: the P-v-T diagrams of most fluids are similar if expressed in reduced variables, which allows, to a certain extent, the generalization of concepts and observations regarding states and properties

Fundamental derivative of gas dynamics: Γ is a fluid thermodynamic property whose value is proportional to the curvature of the isentropes in the P-v plane, i.e., to the slope of c^2

2. FUNDAMENTALS

2.1. Acoustics

The simplest thermodynamic property model allowing for the calculation of vapor-liquid equilibrium and nonideal thermodynamic states is the van der Waals model, which can be rigorously derived using a statistical mechanics approach from an intermolecular potential (McQuarrie 1976, Callen 1985).

Colonna & Guardone (2006) showed that the speed of sound of a polytropic van der Waals fluid c can be written as the sum of the ideal gas sound speed with ideal gas departure terms, namely $c^2 = c^2_{\text{ideal}} + \delta c^2_{\text{rep}} + \delta c^2_{\text{attr}}$. The ideal gas and repulsive forces contributions c^2_{ideal} and δc^2_{rep} decrease with increasing molecular complexity. The ideal gas contribution c^2_{ideal} is related to the free motion and the elastic collisions of the molecules. Therefore, it increases with temperature because the average molecular speed scales with $\sqrt{T}$, and it is independent of v, per the ideal gas assumption of dimensionless (point-wise) molecules interacting only via elastic collisions. Thus, $c^2_{\text{ideal}}(T)$ is constant along isotherms. The repulsive force contribution is a positive contribution to c and depends on the fluid parameter b, the covolume. This contribution tends to infinity as the specific volume tends to the molecular covolume. Attractive long-range forces, depending on the fluid parameter a, increase the compressibility of the fluid, and therefore the attractive force contribution δc^2_{attr} is the only negative term. Attractive van der Waals forces contributing to δc^2_{attr} are solely responsible for the nonmonotonic variation of the sound speed along isotherms, possibly leading to the inversion of the dependence of the speed of sound on the density in isentropic NICFD flows. Remarkably, the contribution of attractive forces is independent of N according to the polytropic van der Waals model. The contribution of the effect of the attractive force is somewhat masked by the two other contributions, which inversely depend on molecular complexity. It follows that, at the same reduced thermodynamic state (a state identified in terms of reduced state variables), the higher the molecular complexity of a fluid, the stronger nonideal gas-dynamics effects are. According to the principle of corresponding states, these considerations are general.

The local speed of propagation of a weak pressure disturbance in a fluid in uniform and possibly nonideal conditions is given by $w = u + c$, where u is the local fluid velocity. Following Thompson (1971), in a simple-wave flow with uniform entropy $\mathrm{d}w = \mathrm{d}u + \mathrm{d}c = \Gamma/(\rho c)\,\mathrm{d}P$, where Γ is the fundamental derivative of gas dynamics,

$$\Gamma = 1 - \frac{v}{c}\left(\frac{\partial c}{\partial v}\right)_s. \qquad 3.$$

Upon compression ($\mathrm{d}P > 0$), the local wave speed increases ($\mathrm{d}w > 0$) only if $\Gamma > 0$, as a result of the increase of both u and c, which becomes greater across an isentropic compression if $\Gamma > 1$. This is the case of, e.g., a polytropic ideal gas, for which $\Gamma = (\gamma + 1)/2$ is constant and greater than 1. If $\Gamma < 1$, the local wave speed qualitatively replicates the wave speed variation in an ideal gas, but it results from the sum of the contributions u and c, which have opposite signs. u increases upon compression and decreases upon rarefaction, but c does the opposite. The existence of single-phase vapor thermodynamic states featuring $\Gamma < 1$ depends on both the thermodynamic state and the fluid molecular complexity (see the sidebar titled Fluid Classes and Molecular Complexity).

FLUID CLASSES AND MOLECULAR COMPLEXITY

The value of Γ depends on molecular complexity and thermodynamic state. A thermodynamic region whose states feature $\Gamma > 1$ exists regardless of the fluid molecular complexity. States with $\Gamma \leq 1$ are possible only in the single-phase nonideal region if the fluid is made of sufficiently complex molecules. Colonna & Guardone (2006) suggested the following classification:

- **Low molecular complexity (LMC) fluids.** $\Gamma_{\min} > 1$ in the single-phase nonideal region. c increases on isentropic compression and decreases on isentropic rarefaction, similarly to polytropic ideal gas flows. Nitrogen, water, carbon dioxide, and other molecularly simple fluids are LMC. LMC substances are used as working fluids in, e.g., supercritical CO_2 power systems and heat pumps (see Section 4).
- **High molecular complexity (HMC) fluids.** Fluids featuring thermodynamic states with $0 < \Gamma < 1$ in the single-phase nonideal region [e.g., according to accurate thermodynamic models, toluene or siloxane MM (hexamethyldisiloxane)]. If the substance is an HMC fluid, the variation of c can be opposite to that occurring in ideal gases: It can decrease upon compression and increases upon rarefaction. All other thermodynamic properties of the fluid evolving within the flow are only quantitatively different from their corresponding variations in dilute gas flows; therefore, the gas dynamics of LMC and HMC fluids is referred to as classical. For example, the working fluids of high-temperature organic Rankine cycle power plants are HMC fluids (see Section 4).
- **Bethe-Zel'dovich-Thompson (BZT) fluids.** Current thermodynamic models, although still insufficiently accurate, predict that fluids made of very complex molecules such as siloxane D_6 or perfluorocarbon PP10 feature a single-phase thermodynamic region whose states are characterized by $\Gamma < 0$, allowing for nonclassical gas dynamics (see Section 2.2). Despite several experimental attempts to verify its existence, no evidence is available yet. BZT fluids are used in laboratory facilities for the scientific investigation of nonclassical gas dynamics (see Section 3.3).

Exemplary T-s diagrams of pure fluids and mixtures belonging to each of these fluid classes are reported in **Figure 2**. Nonideal gas dynamic effects are not limited to flows of molecularly complex fluids. A notable example is the supercritical flow of CO_2, an LMC fluid, or flows of fluids whose thermodynamic states are close to the vapor-liquid critical point.

2.2. Finite-Amplitude Nonlinear Waves

Considering an unsteady 1D wave, if $\Gamma > 1$, the local wave speed w across a compression increases; therefore, over a sufficiently long time, the compression profile steepens to form a compression shock, which in turn causes the entropy to increase. On the contrary, the wave speed across a rarefaction diminishes, so the wavefront spreads over time and propagates isentropically. This wave propagation mode is qualitatively the same as that occurring for ideal gas flows, while quantitative differences exist due to nonideal thermodynamic effects. If the state of the fluid features $0 < \Gamma < 1$, all flow variables change in the same way as in the case of a fluid with $\Gamma > 1$, with the only exception of the speed of sound, which decreases upon compression and increases upon rarefaction, a nonideal gas dynamic effect. Compressible flows of fluids whose thermodynamic states feature $\Gamma > 0$ are termed classical because waves propagate in a qualitatively similar way as they propagate in ideal gas flows. Conversely, nonclassical gas dynamics may occur in the particular case in which the fluid is in states for which $\Gamma < 0$. Wave propagation is inverted with respect to what happens in classical compressible flows, and phenomena like rarefaction shock waves are admissible. The wave speed diminishes across compression, leading to a wave profile spreading in space over time.

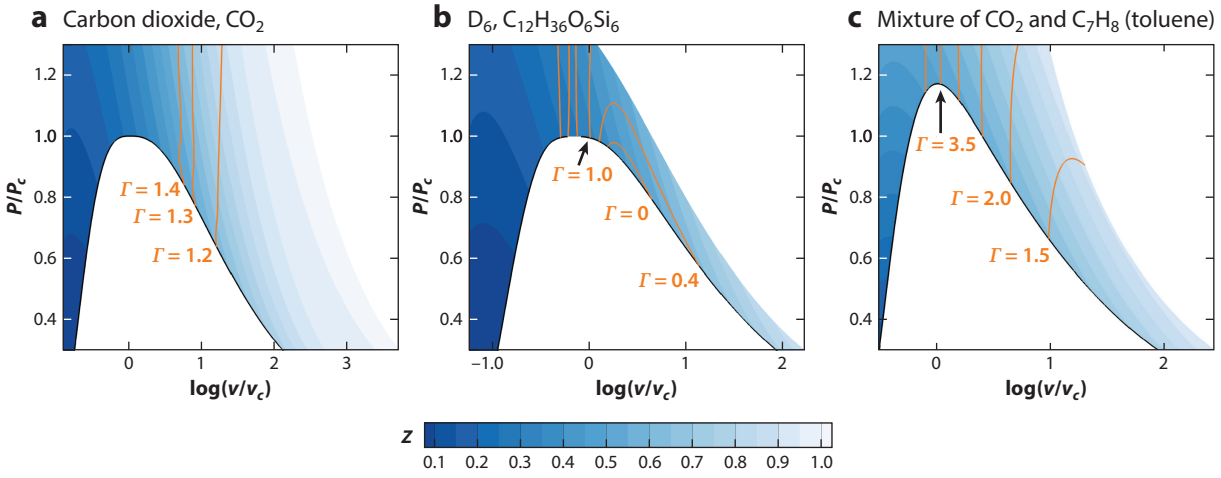

Figure 2

Exemplary isolines of the fundamental derivative of gas dynamics in the pressure-volume thermodynamic plane (reduced variables), where P is pressure, P_c is critical pressure, v is volume per unit mass, v_c is critical volume per unit mass, and Γ is the fundamental derivative of gas dynamics. (*a*) Low molecular complexity fluid. (*b*) Bethe-Zel'dovich-Thompson fluid. (*c*) Equimolar mixture that is a high molecular complexity fluid.

These wave propagation modes are summarized in the sidebar titled From Thermodynamics to Gas Dynamics. In the general case, due to the finite amplitude of the propagating wave, the value of Γ may change as the wave evolves, and different combinations of the propagation modes may be observed.

2.2.1. Prandtl-Meyer waves. Considering steady, adiabatic, and isentropic flows with no discontinuities, the total enthalpy per unit mass h_t is constant along streamlines; hence, the Mach number $M = |u|/c$ is a function of one single variable, for example, the density. Thus, $M = M(\rho)$ and

$$\frac{\rho}{M}\frac{\mathrm{d}M}{\mathrm{d}\rho} = 1 - \Gamma - \frac{1}{M^2} = J(M; h_t, s), \qquad 4.$$

FROM THERMODYNAMICS TO GAS DYNAMICS

Classical gas dynamics	$\Gamma > 1$	$\left(\frac{\partial c}{\partial P}\right)_s > 0$	Compression waves steepen into shock waves; rarefaction waves extend.
	$\Gamma = 1$	$\left(\frac{\partial c}{\partial P}\right)_s = 0$	Acoustic equation of state where P is a linear function of ρ, and c is constant.
	$0 < \Gamma < 1$	$\left(\frac{\partial c}{\partial P}\right)_s < 0$	The speed of sound decreases across an isentropic compression.
Acoustic gas dynamics	$\Gamma \sim 0$	$\left(\frac{\partial c}{\partial P}\right)_s < 0$	Finite-amplitude waves propagate without distortion: No shock waves can form.
Nonclassical gas dynamics	$\Gamma < 0$	$\left(\frac{\partial c}{\partial P}\right)_s < 0$	Rarefaction waves steepen to form rarefaction shock waves; compression waves spread out. This is possible in the vapor phase of Bethe-Zel'dovich-Thompson fluids.

where both b_t and s are constant parameters. For a polytropic ideal gas $\Gamma > 1$ and the quantity J is thus negative, and the M monotonically increases over expansions, e.g., across a centered Prandtl-Meyer expansion fan. If fluid thermodynamic properties are nonideal, the flow evolution strongly depends on the upstream state, a nonideal thermodynamic effect (Wheeler & Ong 2013). Moreover, nonideal gas dynamic effects may occur. For HMC fluids, if fluid states feature $0 < \Gamma < 1$, J can be positive in the supersonic regime and M across an isentropic Prandtl-Meyer expansion wave decreases. Because M and Γ vary along the process, a nonmonotonic M profile may occur. If the fluid is BZT and if a flow occurs with the fluid featuring states with $\Gamma < 0$, a nonmonotonic variation of M along the process may occur even if the flow is subsonic (Cramer & Best 1991, Romei et al. 2020).

2.2.2. Nonideal oblique shock waves. In addition to the nonideal dependence of the shock polar on upstream conditions, another nonideal feature is the discontinuous increase of M across the shock (Vimercati et al. 2018a). Weak oblique shocks from upstream states featuring $J > 0$ are necessarily nonideal oblique shocks. Moreover, due to the effect of the entropy increase, nonideal oblique shocks can occur from upstream states characterized by $J < 0$, although it is still required that $J > 0$ along the shock adiabat connecting the upstream and downstream states. The stability of nonideal shocks is discussed by Vimercati et al. (2018a).

2.2.3. Nonclassical gas dynamics. Flows of BZT fluids may exhibit characteristics that are opposite to those of flows that have been termed classical. In particular, isentropic rarefaction waves can steepen to form nonclassical rarefaction shock waves (Bethe 1942, Zel'dovich 1946, Thompson & Lambrakis 1973, Kluwick 2001). In the literature, the portion of the thermodynamic space of a fluid enclosing states whose Γ is negative is often referred to as the nonclassical gas dynamics region or inversion region.

Moving from the general theory of Liu (1976) and Menikoff & Plohr (1989) for a substance whose thermodynamic properties are modeled with an arbitrary equation of state (EoS), Zamfirescu et al. (2008) demonstrated the existence and uniqueness of the solution of the Riemann problem for fluids in nonideal thermodynamic states, including for nonclassical flows. The solution exists, and it is unique provided that the coefficient of thermal expansion is positive, $\beta = \partial v(T,P)/\partial T/v > 0$, and provided that $\partial Z(T,v)/\partial T \geq 0$. This is the case in the dense vapor and supercritical thermodynamic regions, as it can be verified using appropriately accurate thermodynamic models. Note that $\beta < 0$ only in exceptional cases, e.g., for water at the freezing point. Conditions for admissibility and existence of rarefaction shock waves are discussed in detail by Thompson & Lambrakis (1973), Menikoff & Plohr (1989), Kluwick (2001), and Zamfirescu et al. (2008), including the equilibrium within the shock layer. The stability of the multidimensional shock front was studied by Bates & Montgomery (1999) and Vimercati et al. (2018b).

An interesting feature of nonclassical compressible flows is a consequence of the finite size of the $\Gamma < 0$ region, which may result in the wave states crossing the $\Gamma = 0$ locus during the wave evolution. Crossing the $\Gamma = 0$ locus results in losing the genuine nonlinearity of the acoustic characteristic fields (Menikoff & Plohr 1989). Loss of genuine nonlinearity results in the admissibility of mixed wave propagation, with, e.g., a portion of a compression wave evolving as a classical shock wave followed by a nonclassical isentropic continuous compression. Postshock sonic and preshock sonic shock waves are also admissible, as well as double-sonic shocks with sonic conditions ahead of and past a finite-amplitude shock wave. The nonclassical gas dynamics of mixtures was treated by Guardone et al. (2014). Nonclassical oblique waves and wave interactions were discussed in detail by Vimercati et al. (2018b, 2020).

2.2.4. Nonideal flows at the critical point. Nannan et al. (2014) analyzed the possibility of observing nonideal and nonclassical gas dynamic effects in flows occurring with fluid states near

Nonideal oblique shock: shock that causes an increase in the Mach number across the wave

Mixed wave: loss of genuine nonlinearity across the $\Gamma < 0$ region possibly results in mixed waves, e.g., triple waves composed of two continuous smooth rarefactions embedding a double-sonic rarefaction shock wave

Sonic shocks: if flow states cross the $\Gamma = 0$ curve, pre- and postshock sonic states are admissible; the pre- and postshock states are sonic in double-sonic shocks

the critical point of pure substances, regardless of their molecular complexity. In the vicinity of the vapor-liquid critical point, an analytical model cannot correctly predict the variation of thermodynamic properties, and so-called scaling laws apply. By approaching the vapor-liquid critical point from the single-phase vapor region, scaling laws predict $\Gamma \to \infty$ for all fluids. On the contrary, if the critical point is approached from the two-phase region, $\Gamma \to -\infty$, theoretically allowing for nonclassical gas dynamic effects in flows whose thermodynamic states cross the critical point region.

Eckert number: $Ec = \frac{u_\infty^2}{c_{p_\infty} T_\infty}$, where $u_\infty, c_{p_\infty}, T_\infty$ are the flow velocity, isobaric specific heat, and free-stream static temperature; for an ideal gas it reduces to $(\gamma - 1)M_\infty^2$

Chapman–Rubesin parameter: $C_w = \frac{\mu_w \rho_w}{\mu_\infty \rho_\infty}$, where μ_w, ρ_w and μ_∞, ρ_∞ are the density and dynamic viscosity at wall and free stream

2.3. Laminar Flows

NICFD effects on boundary layer quantities can be analyzed by means of the usual nondimensional quantities characterizing the boundary layer equations, i.e., *Re*, *Pr*, and the Eckert number *Ec*, which is related to both flow compressibility and molecular complexity. While variations of *Re* and *Pr* with the fluid state only entail quantitative changes of the boundary layer characteristics, variations of the Eckert number may lead to trends that are specific to a class of fluids.

Investigations about unperturbed laminar boundary layers of nonideal flows of BZT fluids on a flat plate were first performed by Kluwick (1994). For a fluid in an arbitrary thermodynamic state, $Ec = \mathcal{O}(M_\infty^2 \delta)$, where $\delta = R/c_v$ and M_∞ is the free-stream Mach number. Therefore, contrary to what holds for boundary layer flows of simple-molecule fluids in the ideal gas state, for which $Ec = (\gamma - 1)M_\infty^2$ and $Ec = \mathcal{O}(M_\infty^2)$, in boundary layers of flows of fluids in nonideal thermodynamic states, the condition $Ec \to 0$ does not require that $M_\infty^2 \to 0$. For $Ec \to 0$, the thermal and kinetic flow fields are decoupled, the boundary layer is almost isochoric and isothermal, and the viscous dissipation becomes insensitive to compressibility effects at all Mach regimes (Cramer et al. 1996, Pini & De Servi 2020). HMC fluids are characterized by low values of δ, while, for low molecular complexity (LMC) fluids, $\mathcal{O}(\delta) = 1$. Remarkably, for the viscous flow of fluids made by complex molecules, compressible effects are less relevant. Ideally, for $\delta \to 0$, the specific heat is so large that the temperature does not change within the boundary layer. Moreover, in addition to the isobaric conditions in the normal direction, a well-known result of Prandtl's boundary layer theory, the variation of the density and of any other thermodynamic variable is very small.

The skin friction coefficient C_f and the dissipation coefficient C_D highlight distinctive features of boundary layer flows of HMC and LMC fluids in the nonideal regime. Deviations from the Blasius value of the skin friction occur if compressible effects come into play or, more specifically, if the Chapman–Rubesin parameter deviates from unity (Cramer et al. 1996).

The validity of classical scaling laws for the skin friction coefficient in case of zero-pressure gradient laminar boundary layers was investigated by Cramer et al. (1996). LMC and HMC fluids in the dilute and dense vapor regimes were considered. Numerical calculations revealed that close to the vapor-liquid critical point standard scaling laws do not hold due to the strong variation of fluid thermophysical properties within the boundary layer. As expected, in the case of flows of complex-molecule fluids, deviations are weaker because frictional heating and the associated temperature variation across the boundary layer tend to decrease. Similar findings were obtained by Pini & De Servi (2020), who investigated the impact of NICFD effects on the value of the dissipation coefficient C_D related to the laminar boundary layer over a flat plate.

The effect of the adverse pressure gradient on boundary layer characteristics was examined by Cramer et al. (1997) and Kluwick (2004). The response of a compressible boundary layer of a fluid made of simple molecules subject to an adverse pressure gradient due to shock wave impingement can be largely different depending on the thermodynamic conditions of the undisturbed flow. Marginal separation can occur if the fluid is in near-critical or supercritical conditions, as opposed to a well-developed separation in dilute gas conditions. For an HMC fluid in thermodynamic conditions for which $\Gamma < 1$, boundary layer separation can also occur further downstream. For

example, Kluwick (2004) showed that the variation of M_∞ in the streamwise direction, which follows the variation of Γ due to the change of fluid thermodynamic state, can greatly affect the flow characteristics and that it is possible to reduce, or even suppress, separation induced by adverse pressure gradients for all fluids in nonideal conditions.

2.4. Instabilities in Wall-Shear and Free-Shear Laminar Flows

At low Mach number, the mechanism of transition is driven by viscosity and is related to Tollmien–Schlichting instabilities above the critical Reynolds number. At higher speed, compressibility effects dampen the growth rate of the perturbations and considerably increase the stability of the base flow. Ren et al. (2019b) showed that, in case of flows of CO_2 in the supercritical state, nonideal thermodynamic effects enhance boundary layer stability over adiabatic walls, particularly for high values of Ec, i.e., up to 0.2 ($M_\infty \leq 2$). The results of analysis based on linear stability theory were substantially in agreement with those obtained with direct numerical simulation (DNS). The same characteristics can be observed for flows in subcritical thermodynamic states, where CO_2 is a compressible liquid. However, the CO_2 flow is highly unstable if the fluid is in transcritical states close to the critical point, with the appearance of a new unstable mode. In this case, friction heating causes large density perturbations as a result of the transition between liquid-like and gas-like states within the boundary layer due to the thermodynamic states crossing of the Widom line. Destabilization of laminar jet flows of fluids in transcritical thermodynamic states as a result of the larger velocity fluctuations has also been observed by Sharan & Bellan (2021).

If the fluid is in supercritical conditions and its states cross the Widom line, the transition from liquid-like to gas-like states is made evident by large gradients of thermodynamic and transport properties. These large variations have been found to promote instabilities in Rayleigh–Bénard convection, swirling jet flows, channel flows and boundary layers of pure fluids (Ly et al. 2018, Ren et al. 2019b), and binary mixtures (Ly & Ihme 2022). Transcritical effects also foster laminar-to-turbulent transition in Poiseuille flows (Ren et al. 2019a). Gloerfelt et al. (2020) studied the stability of adiabatic compressible boundary layers of fluids made of complex molecules in states belonging to the $\Gamma < 0$ and $\Gamma < 1$ thermodynamic regions. The authors concluded that the large value of the specific heat is the driving factor inhibiting the thickening of the boundary layer by friction heating, leading to a dampening of the perturbations and to the enhancing of flow stability. For HMC fluids in the dilute gas limit, similar conclusions could be drawn. A remarkable feature of the base flow of HMC fluids is also the absence of a generalized inflection point, which suggests that, at least for adiabatic flows, the primary mechanism of transition is essentially viscous up to Mach numbers featured in practical applications.

2.5. Turbulence and Heat Transfer

Turbulence kinematics and dynamics in compressible flows are much affected by variations of fluid thermophysical properties such as dynamic viscosity, density, and speed of sound (Bradshaw 1977); thus, turbulence characteristics depend on the considered fluid class and thermodynamic state (Tosto 2023) (see **Figure 3**). For example, given that the thermal energy input caused by the dissipation of the turbulent kinetic energy (TKE) at the smallest scales has a larger impact on the variation of thermophysical properties in LMC fluids rather than in HMC compounds, one can expect that the most striking differences between turbulence generated in dilute gas flows and dense-vapor flows occur if the fluid is made of simple molecules. When examining turbulence in the context of NICFD, particular attention must be devoted to distinguishing between effects related to fluid molecular complexity and those due to the nonideal thermodynamic state.

Generalized inflection point: $\frac{\mathrm{d}(\rho \mathrm{d}u/\mathrm{d}y)}{\mathrm{d}y} = 0$, where u, y are the streamwise flow velocity and the direction normal to wall

Turbulent kinetic energy (TKE): for compressible flows $\frac{\overline{\rho u_i' u_i'}}{2\bar{\rho}}$. u_i' is the i-component of the velocity fluctuations (Favre averaging is applied); the rate of decay of TKE is almost insensitive to the type of molecule

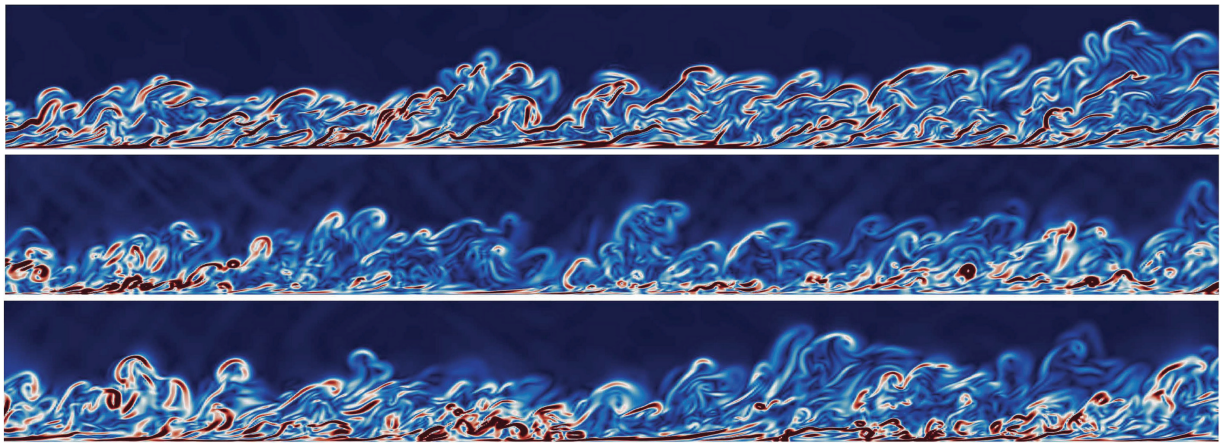

Figure 3

Velocity fluctuations within the zero-pressure gradient turbulent boundary layer over a flat plate for air (*top*) and siloxane hexamethyldisiloxane in ideal (*middle*) and nonideal (*bottom*) thermodynamic conditions. The calculations were performed with a direct numerical simulation solver (Tosto 2023). Figure adapted from Tosto (2023) (public domain).

Sciacovelli et al. (2017) and Duan et al. (2021) researched dense vapor effects on the largest and smallest structures of homogeneous isotropic turbulence for an HMC fluid using DNS. Compared to air, turbulence dynamics is primarily modified by effects related to molecular complexity, while the small-scale dynamics can be significantly influenced by the local variations of the speed of sound, i.e., it can be characterized in terms of Γ. Of particular relevance is the fact that global flow kinematic properties are barely affected by the type of fluid molecules.

Vadrot et al. (2021) reported a numerical comparison of the turbulent characteristics in a compressible mixing layer for air and for a dense vapor of an HMC fluid in different thermodynamic conditions. The most remarkable outcome is that the growth rate of the mixing-layer momentum thickness is similar, and it becomes larger for the HMC fluid only if strong compressibility effects come into play. However, at the smallest scales, turbulence dynamics is substantially different, possibly highlighting the need for ad hoc subgrid scale models for large eddy simulation (LES). Moreover, the change of the thermodynamic state has a negligible impact on the temporal evolution of the mixing layer. This is possibly due to the dominant effects of molecular complexity.

In wall-bounded flows, turbulence is primarily modulated by strong wall-normal gradients of density and viscosity, which in turn affect the speed of sound, the local Mach number, and the local Reynolds number. Strong variations of thermophysical fluid properties can occur in LMC fluids at supercritical or dense vapor states. Either friction heating or heat transfer can cause highly nonlinear density and viscosity changes in these fluids, which in turn affect turbulence. The pioneering studies of Pecnik & Patel (2017) demonstrated that leading-order effects of variable properties on turbulence can be characterized in terms of semilocal Reynolds number, while the classical law of the wall can be retrieved, albeit within a certain degree of accuracy in the log region, by applying the transformation to the velocity distribution proposed by Trettel & Larsson (2016). The observation that the flow characteristics of an HMC fluid in dense vapor or ideal gas states vary similarly to how they vary for incompressible flows would also apply, from a macroscopic viewpoint, to turbulent quantities. This has been confirmed by Sciacovelli et al. (2020) by means of DNS, as they show that integral quantities such as C_f or the Nusselt number Nu can be accurately predicted using correlations developed for incompressible flow even at very high Mach numbers, as the state of the boundary layer is almost insensitive to friction heating. Correct

scaling of the velocity distributions can be obtained for these fluids by means of, e.g., the Trettel and Larsson transformation. Compressibility effects can be appreciated only by inspecting the pressure and density fluctuations, which have been found to be of the same order of magnitude of those occurring in air flows.

Improvements of existing eddy viscosity models applicable to wall-bounded nonideal turbulent flows require that the effects of strong wall-normal gradients of density and viscosity are accounted for in the TKE equation (Pecnik & Patel 2017, Otero et al. 2018). Using the semilocal Reynolds number, Otero et al. (2018) derived an alternative formulation of the TKE equation, which can be used in conjunction with eddy viscosity turbulence models, and adapted five eddy viscosity turbulence models to account for variable thermophysical properties. The authors showed that the original Spalart-Allmaras (SA) model provides accurate estimations of the velocity and temperature distribution also in case of variable-property turbulent flows and, as such, should be used for simulating nonideal compressible flows. However, other common turbulence closures can provide results that are in qualitative agreement with the results of DNS of nonideal flows of HMC fluids and can therefore be adopted if performing Reynolds-averaged Navier-Stokes (RANS) computations (Sciacovelli et al. 2018). The recent study by Schuster et al. (2023), in which the authors assessed density and compressibility corrections to the SA and SST-$\kappa\omega$ turbulence models, and that of Tosto (2023) corroborate the outcome that those model improvements have a negligible impact on the results of wall-bounded simulations of HMC fluid flows. The variation of fluid thermophysical properties can substantially affect heat transfer in supercritical fluid flows (Peeters et al. 2016, Kawai 2019), and a proper value of the turbulent Prandtl number Pr_t is needed for the accurate modeling of heat transfer effects with RANS solvers (Sciacovelli et al. 2018).

2.6. Inviscid Nozzle Flow

Cramer & Best (1991) examined steady isentropic flows in the nonideal regime and pointed out that the Mach number does not necessarily increase monotonically with decreasing density if the thermodynamic states of the fluid feature $\Gamma < 1$, which is possible for HMC and BZT fluids. In nonclassical nozzle flows, the number of sonic points may increase from one to three, resulting in the occurrence of rarefaction shocks in the convergent and divergent sections of the nozzle (see Chandrasekar & Prasad 1991, Cramer & Fry 1993, Kluwick 1993). Thompson (1971) was the first to investigate the role of the sign of Γ in these paradigmatic flows, demonstrating that an antithroat is required to accelerate the fluid to supersonic speed.

Figure 4 depicts the variation of the area distribution and Mach number along the nozzle centerline related to exemplary simulations of supersonic nozzle expansions of fluids representative of the LMC, HMC, and BZT classes. **Figure 4*a*** shows the nozzle design for CO_2 operating in nonideal and ideal conditions, together with the variation of the Mach number. Differences with respect to ideal gas behavior are limited to nonideal thermodynamic effects, and the solution is qualitatively similar to that obtained on the basis of the dilute gas approximation. **Figure 4*b*** displays the same chart for fluid MM (hexamethyldisiloxane). In addition to nonideal thermodynamic effects resulting in a larger nozzle exit area for the same exit Mach number, a nonideal gas dynamic phenomenon is apparent: the nonmonotonic Mach number profile in the divergent section of the nozzle, where $J > 0$, which is possible only for HMC and BZT fluids. **Figure 4*c*** displays nozzle design for a BZT fluid (D_6), in which, for $J < 0$, a nonmonotonic Mach trend in the converging section of the nozzle can occur.

Given the dependence of Γ on total conditions, the flow evolution varies if the reservoir or total conditions are changed, a feature of nonideal flows. Qualitative changes of the sound speed and Mach profiles quantitatively affect the variation of the density, pressure, and velocity, which, however, all preserve the qualitative features of ideal flows. Romei et al. (2020) studied the

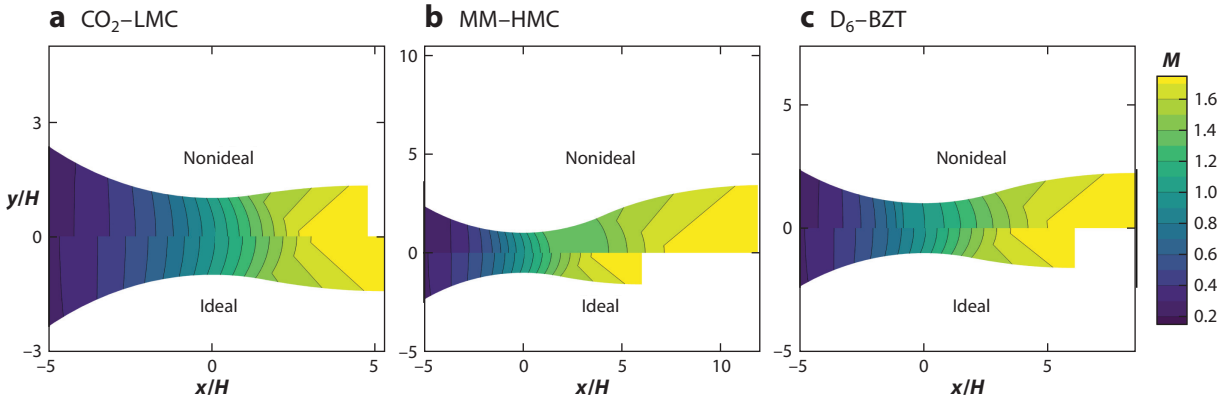

Figure 4

Exemplary supersonic nozzle designs for fluid representative of the (*a*) LMC, (*b*) HMC, and (*c*) BZT classes assuming nonideal (*top*) and ideal (*bottom*) thermodynamic models of the fluid, where H is half of the throat height and M is the Mach number. Abbreviations: BZT, Bethe-Zel'dovich-Thompson; HMC, high molecular complexity; LMC, low molecular complexity; MM, siloxane hexamethyldisiloxane. Figure adapted from Zocca et al. (2023).

dependence of the flow quantities on total conditions and showed that for MM, if the fluid at the inlet is in a nonideal thermodynamic state, a larger area ratio A/A_{th} is required to accommodate the larger variation of the volume flow rate. Conti et al. (2021) showed how the critical pressure ratio P^*/P_t in sonic conditions strongly depends on the thermodynamic nonideality of the fluid states and the flow path is governed by the evolution of values and gradients of both the compressibility factor Z and the fundamental derivative of gas dynamics Γ. For HMC fluids, P^*/P_t increases with nonideality for $0.5 \leq Z_t \leq 0.9$. The same trend was observed experimentally by Spinelli et al. (2018). If the nonideality of the fluid at the inlet is even stronger ($Z_t < 0.5$), due to considerable gradients of both Z and Γ, the variation is no longer monotonic, with a possible strong reduction of the critical ratio. For simple-molecule fluids, deviations of the pressure distribution with nonideality are smaller, and different fluids do not exhibit a common trend. Guardone & Vimercati (2016) derived an exact procedure for the solution of the nozzle flow equations for the general case of a fluid with nonideal thermodynamic properties, including shock waves, and listed all possible solutions to the nozzle expansion problems for LMC, HMC, and BZT fluids and their dependence on stagnation conditions. (See the sidebar titled Nonideal Compressible Fluid Dynamic Effects.)

3. MODELS AND METHODS

3.1. Numerical Methods for Flow Simulations

The generalization of a flow solver from ideal to nonideal conditions is not trivial. The use of complex fluid models coupled with the flow governing equations, either implemented in external libraries or directly coded into the flow solver (see Section 3.2), significantly impacts the numerical solution stability and computational cost. In ideal gas CFD solvers, the internal energy and the enthalpy depend on temperature only and are often used interchangeably; in NICFD, thermodynamic properties depend on two thermodynamic variables. The computational time required by an NICFD simulation can increase by as much as two orders of magnitude with respect to the equivalent simulation of an ideal gas flow. Acceleration techniques, including look-up tables (LUTs), can reduce the computational effort (see Section 3.2). When selecting the

NONIDEAL COMPRESSIBLE FLUID DYNAMIC EFFECTS

Nonideal thermodynamic effects are effects caused by nonideal thermodynamic properties that do not cause the qualitative departure of the flow characteristics from those of ideal gas flows. However, property values and variations of flow quantities along processes are quantitatively different from those of an ideal gas flow. For example, for a specified expansion ratio, the Mach number at the outlet of a supersonic nozzle depends on total thermodynamic conditions, whereby it depends on the geometry and on γ only if the expanding fluid is an ideal polytropic gas.

Nonideal gas dynamic effects are effects caused by nonideal thermodynamic properties that result in qualitatively different flows if compared to ideal gas flows. Examples are the nonmonotonic variation of the Mach number across expansions, classical nonideal oblique shocks, nonclassical rarefaction shock waves and mixed waves, and the incompressible-like flow within the boundary layer if fluid thermodynamic states are not in the proximity of the Widom line or the critical point. These effects, therefore, occur in both classical and nonclassical compressible flows.

thermodynamic property model, one must also consider the specific needs of computational fluid dynamics (CFD) software. For example, the evaluation of the advective-flux Jacobian required by implicit CFD schemes entails the evaluation of the pressure derivatives with respect to the specific internal energy and the density (Colonna & Silva 2003).

Several RANS solvers, including both open-source (Vitale et al. 2015, Qi et al. 2022) and commercial (Romei et al. 2020) codes based on well-established finite volume schemes, are available. Colonna & Rebay (2004) reviewed early efforts to simulate NICFD flows that relied on various methods ranging from finite differences to finite volume schemes, including approximate Riemann solvers generalized to so-called real gas flows. The generalization of numerical methods originally devised for ideal gas flows must account for the different mathematical properties of the governing equation. First, the advective flux function in the Navier-Stokes equation is no longer a homogeneous function of degree one, resulting in the Jacobian matrix of the fluxes dependence on the density in addition to the velocity and total enthalpy (Rinaldi et al. 2015). This requires, e.g., the explicit computation of an average density value in the Roe linearization process (Guardone & Vigevano 2002) or the use of a non-Jacobian form of the Roe matrix (Cinnella 2006). The loss of genuine nonlinearity possibly occurring in flows of BZT fluids, and the consequent occurrence of nonclassical phenomena (Section 2.2.3), is an additional challenge that might prevent the straightforward application of numerical schemes devised for ideal gases. A notable example is the use of techniques for enforcing the fulfillment of the entropy condition in shock-capturing schemes. Entropy fixes based on artificial viscosity, such as the Harten and Hyman fix, have been successfully applied to the solution of NICFD computations (Guardone & Vigevano 2002). The extension to the NICFD case of simplified flow solution methods, such as the method of characteristics (Zocca et al. 2023), quasi-1D solvers (Vimercati & Guardone 2018), or through-flow methods (Pini et al. 2015), requires addressing similar issues. Vitale et al. (2015, 2020) reviewed boundary conditions for the simulation of NICFD flows. It is common to experience that correctly initializing NICFD simulations can be very time-consuming. A systematic study on strategies to set up the initial flow field is lacking in the literature.

The discretization of advective fluxes in LES and DNS solvers for NICFD is often based on high-order central-difference or finite-difference schemes with shock-capturing corrections. In this case, the only modification required to adapt a high-order solver developed for ideal gas flows is limited to implementing computationally efficient thermodynamic models. On the contrary, weighted essentially nonoscillatory reconstruction schemes require significant modifications of

the formulation of the numerical fluxes (Duan et al. 2021). Research on the application of LES and DNS models to the simulation of NICFD flows to better understand detailed physical phenomena is particularly active (Sciacovelli et al. 2017, Touber 2019, Giauque et al. 2020). For example, high-fidelity simulations are used to investigate bypass transition and mixing of shear layers. DNS data are instrumental in fine-tuning turbulence models suitable for the simulation of NICFD flows (see Section 2.5). In nonideal flows, low values of the Mach number do not necessarily imply that the flow is incompressible or quasi-incompressible. Methods for the simulation of low Mach number NICFD flows are currently being developed (see, e.g., the study in Re & Abgrall 2022).

Optimization techniques initially developed for ideal flows have been successfully applied to the design of components operating in the nonideal flow regime, such as, e.g., supersonic vanes of ORC turbines (Vitale et al. 2017, Persico et al. 2019). Vitale et al. (2017) applied automatic differentiation tools to devise adjoint NICFD solvers. The automatic differentiation process is not straightforward if external thermodynamic property libraries are involved and proper numerical treatment is needed (Rubino et al. 2021).

The verification and validation of NICFD solvers is a goal not yet fully accomplished due to the scarcity of experimental data and the uncertainty of the operating conditions and models. Uncertainty quantification techniques have been applied to quantify the uncertainty due to thermodynamic models (Razaaly et al. 2019). The possibility of tuning thermodynamic parameters via Bayesian inference from experimental data is discussed by Gori et al. (2020b). The impact of geometrical uncertainties was first assessed by Razaaly et al. (2019). Shape optimization under uncertainty was first carried out by Cinnella & Hercus (2010), including operating conditions and model parameters.

The first validation of a CFD code against experimental data under both numerical and experimental uncertainty was documented recently by Gori et al. (2020a), with experimental data obtained with the test rig for organic vapors (TROVA) facility (see Section 3.3.1). **Figure 5*a*** shows

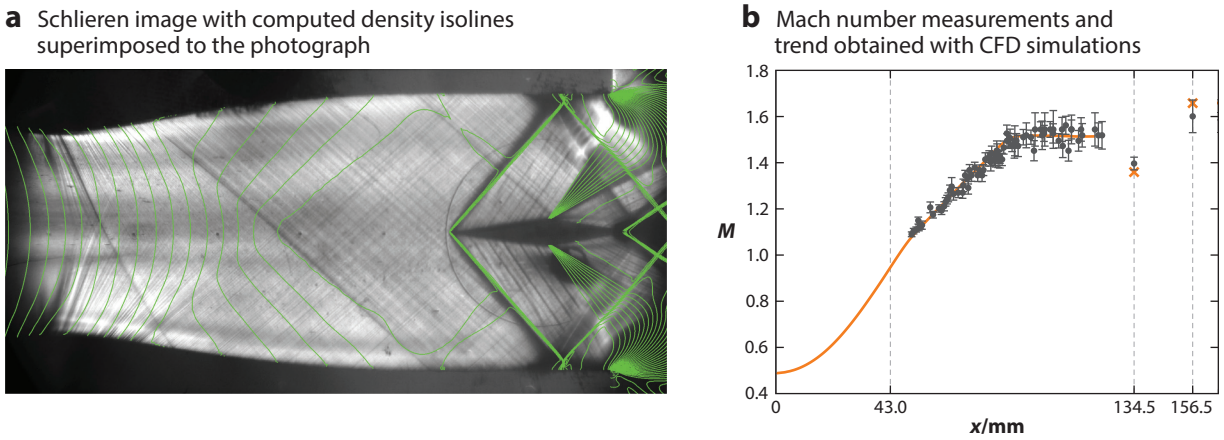

Figure 5

(*a*) Supersonic flow of dense MDM vapor around a diamond-shaped airfoil at the outlet of the converging-diverging nozzle of the TROVA. $\Gamma = 0.92$ upstream of the wedge. (*b*) Comparison of M measurements (*black filled circles*) against CFD simulation results obtained along the centerline of the divergent part of the nozzle: The orange line indicates values up to the leading edge of the diamond-shaped airfoil; the orange × indicates single point values after the oblique shock wave and after the expansion fan. Uncertainties of measured data are also indicated. Abbreviations: CFD, computational fluid dynamics; M, Mach number; MDM, octamethyltrisiloxane; TROVA, test rig for organic vapors. Figure adapted from Zocca (2018) (public domain) and Zocca et al. (2019) (CC BY 4.0).

a schlieren image of the supersonic flow around a diamond-shaped airfoil, with superimposed density isolines from numerical simulations. The fluid is accelerated from nonideal conditions (total conditions are $T_t = 277°C$, $P_t = 8.7$ bar, $\Gamma_t = 0.61$, $Z_t = 0.7$) to Mach 1.6. **Figure 5*b*** displays the indirect measurements of the Mach number obtained from the angle of the Mach lines made evident by schlieren photographs (Cammi et al. 2021). The flow field, with leading and trailing edge oblique shocks and a Prandtl-Meyer fan at the maximum thickness point, was simulated with a good degree of accuracy.

3.2. Modeling of Fluid Thermodynamic and Transport Properties

3.2.1. Thermodynamic property modeling. The accuracy and consistency of property models are particularly relevant in NICFD because theoretical formulations and numerical simulations of flows strongly depend on the accurate estimation of derivatives of primary properties (e.g., c and Γ). Thermodynamic models are based on EoSs expressing relations between properties. Forms of EoS models are explicit either in the specific Helmholtz energy, $a = a(T, v)$, or in pressure, $P = P(T, v)$ (see, e.g., Reynolds & Colonna 2018, chapters 6 and 8). These models must be bounded by conditions expressing limits pertaining to the existence of the molecule, like, e.g., the limit of thermal stability of a fluid.

Helmholtz-based EoS models (Span 2000) are semiempirical: They are based on some physical concepts and thermodynamic bounds but result from the complex constrained regression of a large amount of accurate experimental thermodynamic property measurements (e.g., PvT data, c data). The accuracy of these multiparameter EoS models is correlated to the number of parameters: They are classified as reference or technical models.

A large variety of cubic equation of state (CEoS) models usually expressed as $P = P(T, v)$ are available; also see the review by Lopez-Echeverry et al. (2017) for the accuracy of CEoSs. They have a theoretical basis, being all derived from the van der Waals model; data exist for many fluids and can easily be extended to compute mixture properties.

A thermodynamic model valid only for dense-vapor states is the so-called virial EoS. Such a model, often expressed as a Taylor expansion of the compressibility factor, is rather accurate and has a strong theoretical foundation as it can be rigorously derived from statistical thermodynamics theory. However, it is valid only for mildly nonideal states, and fluid data are scarce.

Another family of physics-based models that is now commonly adopted is derived from statistical associating fluid theory (SAFT) (see Gross & Sadowski 2001). The Helmholtz energy is expressed as the sum of contributions due to hard-sphere repulsive interactions, chain formation through bonding of hard spheres, and association of molecules. These contributions are accounted for in terms of molecular parameters, obtained from a description of the molecular potential, whose constants are available in databases or can be obtained from measurements or molecular simulations (so-called ab initio calculations). The accuracy of SAFT models is remarkable, given the small number of parameters they depend on.

Statistical thermodynamics theory is also the rigorous foundation of numerical methods for the calculation of thermodynamic properties (McQuarrie 1976). However, its use in the context of flow simulations is impractical due to the excessive computational cost. Statistical thermodynamics can be used to support the derivation of EoS models, albeit still limited to simple molecules.

Properties of fluid mixtures can usually be calculated with the same EoS models of pure fluids, whereby fluid parameters are related to pure-compound constants by means of so-called mixing rules. Mixing rules are semiempirical relations; therefore, experimental vapor-liquid-equilibrium data are most often needed for fitting. Given the complex interaction between different molecules, the accuracy of mixture property models is lower if compared to that of pure-fluid models.

Forms of EoS models: for a thermodynamic model expressed as $a = a(T, v)$, all other properties can be derived analytically; for $P = P(T, v)$ models, an expression for the ideal gas c_P or c_v is also needed

Thermal stability for a fluid: many flow simulations involve organic molecules at high temperature; the fluid thermal stability must be correctly considered to avoid computing fluid states that cannot exist due to molecule decomposition

Reference model: multiparameter EoS model whose uncertainty (0.01% or 0.1%, depending on the property) is of the same order as that of the highly accurate experimental data used for fitting; available for only a few simple-molecule fluids, e.g., CO_2

Technical model: multiparameter EoS model with uncertainty higher than that of reference models (0.1%) but lower than that of simpler models, e.g., cubic EoS; available for an ever-increasing number of substances

Accuracy of CEoS: the small number of parameters and its functional form prevent CEoS models from being accurate over the entire thermodynamic space; they are inaccurate for states close to the critical point

Accuracy of SAFT models: these models can be more accurate than cubic EoSs and are also suitable for estimating mixture properties; however, they inaccurately predict property variations close to the critical point

Consistent LUT method: given, e.g., P, T, h, with $P = P(T, h)$ and $T = T(h, P)$, one obtains the same pressure with $P = P(T(h, P), h)$; this is ensured only if the pressure and enthalpy satisfy the associated Maxwell relations

Within the context of NICFD, many EoS models have been used for theoretical and numerical studies. The van der Waals model has been adopted in the initial studies on nonclassical gas dynamics and to date for the derivation of theoretical insights. This simple model correctly describes the qualitative variation of properties and allows for analytical developments, although the calculation of properties of dense vapor states is inaccurate. In particular, it largely overpredicts values of Γ.

Colonna & Silva (2003) provided a compendium of all secondary thermodynamic properties needed by implicit RANS flow solvers and their analytical derivation from EoSs in the $P = P(v, T)$ form. In a series of studies, Colonna et al. (2009) demonstrated that several substances of the siloxanes family may be BZT fluids and assessed the possible accuracy of the Γ calculations by comparing the results of evaluations performed with reference and technical EoSs for simple molecules, concluding that technical multiparameter models might more accurately estimate secondary properties of dense vapors if compared to CEoSs, provided that they are fitted on a sufficient number of accurate experimental data. More recently, Castier & Cabral (2012) evaluated Γ for the saturated vapor of approximately 1,800 substances using Peng-Robinson types of CEoS. Especially in the case of complex organic compounds, experimental data are few and the estimation of Γ is affected by large uncertainty, to the point that there cannot be confidence that BZT fluids exist. A first attempt at measuring the speed of sound of a complex organic compound in the dense vapor region was performed by Mercier et al. (2023), but more data for more fluids and with reduced uncertainty would be desirable.

Many of the mentioned models are implemented in software libraries on which CFD software often relies for the computation of needed fluid properties. All these models are based on functions whose dependent variables—i.e., $P(T, v)$ and $a(T, v)$—are different from the variables appearing in the flow motion equations, i.e., primitive or conservative variables. The evaluation of properties therefore requires computationally expensive iterations and, if the phase of the specified state is unknown, also a so-called phase check with lengthy vapor-liquid equilibrium calculations. Among the many methods that can be adopted to reduce computational time, so-called LUT algorithms are the ones most often adopted in both commercial and open-source flow solvers. These algorithms can be classified as consistent or inconsistent (Swesty 1996). Consistency may be relevant for scale-resolved flow simulations, while in the case of RANS simulations, experience showed that the computational performance of the two approaches is comparable. However, a rigorous study on this matter is lacking in the literature (Rubino et al. 2018).

Machine learning techniques are a promising tool to develop computationally efficient surrogate thermodynamic models. Milan et al. (2021) performed a first comprehensive study on the use of a deep feed-forward neural network with appropriate boundary information to calculate the thermophysical properties of a multicomponent mixture for the simulation of supercritical fluid injection. Finally, another emerging technique is based on approximating fluid thermodynamic properties with Chebyshev expansions (Bell & Alpert 2021). So far, the method has been applied to evaluate the vapor-equilibrium properties of pure fluids, demonstrating a very high level of accuracy and a reduction of computational time of two orders of magnitude compared to traditional methods. Extending the method to functions of two independent thermodynamic variables for single-phase calculations should be possible, resulting in fast computations at the cost of memory usage.

3.2.2. Transport property modeling. Transport properties affecting NICFD are viscosity and thermal conductivity (see Sections 2.3 and 2.5). The relevance of the accuracy of transport property models to the simulation of NICFD flows has not been documented yet. A well-established reference for the fundamentals of transport properties computation is *Properties of Gases and Liquids* by Poling et al. (2001) (see chapter 9 for viscosity and chapter 10 for thermal conductivity).

For fluids in the ideal gas state, the simple Sutherland's law for air can be extended to other fluids with appropriate coefficients, while the assumption of constant Prandtl number, generally valid for diluted gases, provides a way to compute the thermal conductivity. If the pressure is low, viscosity and thermal conductivity depend only on temperature.

The effect of pressure on viscosity and thermal conductivity becomes significant for $1 < T_r < 1.5$ and $P > P_c$. At the critical point, both transport properties diverge. The viscosity of a high-pressure vapor depends strongly on density. The pressure dependence of the thermal conductivity of a high-pressure vapor is more complex: It increases with increasing gradient with the state approaching the vapor-liquid critical point.

Several methods to predict dense-vapor or supercritical fluid viscosity were devised and are expressed as the sum of an ideal gas term and a departure function. Poling et al. (2001) recommend the use of the Chung method for the calculation of high-pressure vapor viscosity of both polar and nonpolar compounds over the transport property prediction (TRAPP) method. Errors of the order of a few percent are to be expected, except close to the critical point and for states featuring a density of the same order of magnitude of liquids, whereby the error may be higher. Both the Chung and TRAPP methods have been extended to mixtures, whereby parameters include the dependence on the composition (one-fluid approximation), and the accuracy decreases with respect to pure-fluid models.

The TRAPP method was further developed into extended corresponding state models (Chichester & Huber 2008). Extended corresponding state models can be very accurate, if measurements are available, but are computationally demanding. The residual entropy scaling method is computationally very efficient and simple to implement, and its accuracy can be comparable to that of extended corresponding state models (Bell & Laesecke 2016).

In recent years, Novak (2011) developed an entropy scaling model for viscosity. Lötgering-Lin & Gross (2015) further developed the concept, using the perturbed-chain polar SAFT EoS for the estimation of the residual entropy. Variants of the entropy scaling approach are based on the use of different EoSs, e.g., Helmholtz-based multiparameter (Bell & Laesecke 2016). Much research is also devoted to extending entropy scaling models to calculate transport properties of mixtures (Yang et al. 2022).

Another development in the field is the friction theory of Quiñones-Cisneros et al. (2000), whereby a classical mechanic model of viscosity is obtained by assuming that viscosity is the result of momentum exchange between layers moving at different velocity and interacting as van der Waals molecules. Quiñones-Cisneros et al. (2021) very recently extended this model to compute thermal conductivity and provide a clear summary of friction theory for viscosity, current status, and measurement techniques for thermal conductivity.

Entropy scaling: the residual entropy correlates with the variation of transport properties in dense states; molecular simulations corroborate this observation, except for molecules with complex intermolecular potential (e.g., water and alcohols)

3.3. Experimental Techniques

3.3.1. Test facilities. Arguably, the first document reporting NICFD experiments is the PhD thesis of Duff (1966). Professor Thompson and colleagues studied liquefaction shocks in dense organic vapors of so-called retrograde fluids (Dettleff et al. 1979). Kutateladze et al. (1987) were the first to perform experiments aimed at proving the existence of rarefaction shock waves. Their results were later confuted (see, e.g., Nannan et al. 2013). Bier et al. (1990) extended Duff's research. Anders et al. (1999) adopted SF_6 as the working fluid of a wind tunnel for transonic aerodynamics experiments. The second attempt to detect a rarefaction shock wave was initiated by Fergason et al. (2003) but failed due to the thermal decomposition of the working fluid. Lettieri et al. (2015) conducted supersonic supercritical CO_2 expansion/condensation experiments. An inconclusive assessment about the acceleration of rarefaction waves in the dense vapor of D_6 is reported by

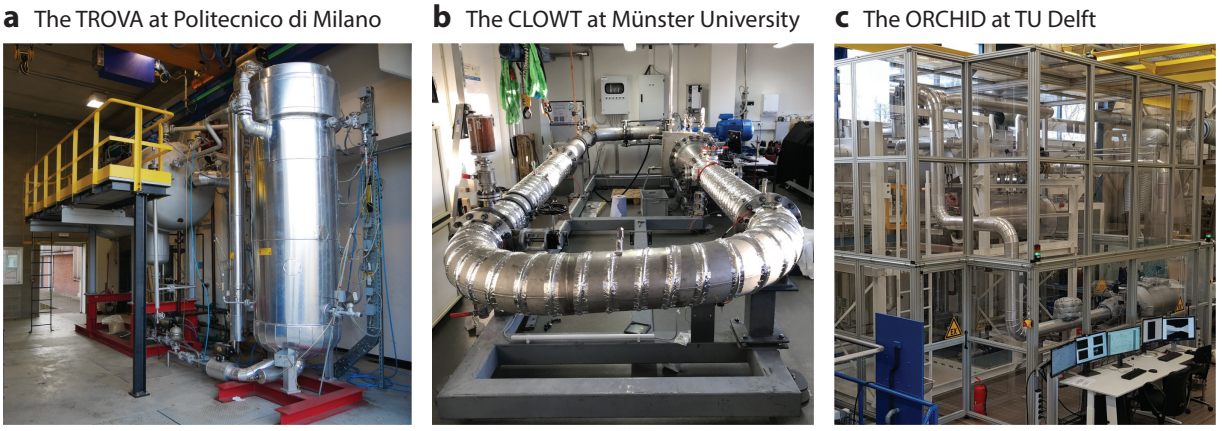

Figure 6

(*a–c*) Exemplary experimental setups currently operated to investigate NICFD flows. Abbreviations: CLOWT, closed loop organic vapor wind tunnel; NICFD, nonideal compressible fluid dynamics; ORCHID, organic Rankine cycle hybrid integrated device; TROVA, test rig for organic vapors; TU Delft, Delft University of Technology.

Mathijssen et al. (2015). Recent developments of this research are reported by Chandrasekaran (2023).

Currently operated NICFD setups include those devoted to the study of fundamental fluid mechanics aspects [these are briefly reviewed here (see, e.g., **Figure 6**)] and those employed to study specific industrial applications. The TROVA at Politecnico di Milano (**Figure 6*a***) is a blow-down facility commissioned in 2013, while NICFD experiments started in 2015 (Spinelli et al. 2017). Maximum operating pressure and temperature are 50 bar and 400°C. The test section can be adjusted to obtain paradigmatic compressible flow fields, a calibration section for NICFD instrumentation, and used to test components of industrial interest (e.g., turbine blade cascades). The total conditions at the inlet of the test section are time dependent, but a sequence of quasi-steady conditions can be obtained. The test section is equipped with one-sided optical access, pressure probes, taps for total and static pressure measurements, and miniaturized thermocouples for total temperature measurements. The facility is designed to operate with various working fluids and can generate flows ranging from subsonic to highly supersonic. Supersonic expansions of dense MDM vapor through a De Laval nozzle affected by appreciable nonideal effects were studied by measuring the static pressure and supersonic Mach number along the nozzle centerline (Spinelli et al. 2018). The local Mach number was obtained by numerically processing schlieren images displaying Mach lines that form due to the roughness of the nozzle metal surfaces (Cammi et al. 2021). The local pressure ratio and Mach number measurements depend on the inlet total state. Successively, Zocca et al. (2019) investigated steady oblique shock waves forming due to the interaction with a diamond-shaped airfoil. The measurements confirm the predictions of shock wave theory for 2D steady flows if adapted to the NICFD case. Experimental data confirm the nonideal dependence of the pressure ratio across the shock on stagnation conditions. A laser Doppler velocimetry (LDV) system, including a novel seeding device, was employed for measurements of subsonic and supersonic flows (Gallarini et al. 2021). The velocity field was compared with the result of flow simulations and with velocities computed from pressure and temperature measurements. In both cases, the maximum deviation between measured and computed velocities is 6.6%. MM was also the working fluid of experiments aimed at measuring total pressure losses across shocks (Conti et al. 2022b). A total pressure probe was inserted at various positions in the diverging part of the

nozzle at flow conditions that are representative of the operation of the first stage of an ORC turbine. Measured shock losses were compared with the results of numerical solutions of the conservation equations across a normal shock. The difference between measured and calculated values is always lower than 2%. It was documented that flow nonideality affects shock intensity: Even at the mildly nonideal conditions of the experiment, the shock is considerably stronger than the shock that would form in an ideal gas flow with the same preshock Mach number.

The closed-loop organic vapor wind tunnel (**Figure 6*b***) commissioned at Münster University of Applied Sciences in 2019 is a Göttinger-type facility (closed-loop vapor cycle) aimed at generating continuous compressible subsonic and transonic flows with low turbulence levels. A compressor provides pressurization, while the temperature at the inlet of the test section is controlled with a finned heat exchanger. The setup was designed for the working fluid Novec 649, $CF_3CF_2C(O)CF(CF_3)_2$. The initial experiments were aimed at characterizing the test section in terms of turbulence and at demonstrating the use of hot wire anemometry in organic vapor flows. Recently, a study on a circular cylinder in the cross-flow of dense vapor and air was carried out (Reinker et al. 2021). Two flow regimes were considered, one at almost incompressible conditions ($M < 0.4$) and another in compressible subsonic conditions ($0.4 < M < 0.8$). The nonideality of the flow was mild ($0.87 < Z < 1$). Information on the surface pressure field was obtained using time-averaged pressure measurements and was used to calculate the drag and base-pressure drag coefficient. Comparing the organic fluid flow features with those of the airflow allowed the assessment of the influence of nonideality, molecular complexity, and flow configuration for these operating conditions. Data showed that nonideal gas dynamic effects have little influence on overall drag and only influence the flow field locally.

The ORC hybrid integrated device (Head 2021) (**Figure 6*c***) was commissioned at Delft University of Technology (TU Delft) in 2018. It implements a regenerated Rankine cycle that can feed two test sections, alternatively, with dense organic vapor. One test section is for fundamental studies and currently consists of a convergent-divergent nozzle with multiple optical access. The other is a test bench for high-speed ORC turbines. The limiting operating conditions for the organic vapor at the inlet of the test section are $T = 400°C$ and $P = 25$ bar. The organic vapor is heated via a thermal oil loop by an electric furnace delivering a maximum thermal power of 400 kW. It was designed to be able to accommodate various working fluids and is explosive atmospheres certified. The first experimental campaign (Beltrame et al. 2021) was dedicated to the generation of data for the validation of CFD codes. Mach waves generated by the supersonic expansion of MM and recorded in schlieren images were used to calculate the local Mach number along the centerline. The thermodynamic state of the fluid at the nozzle inlet was close to the critical point. The maximum deviation between the measured and the calculated Mach number is 4.4%. Recently, the angle of a shock wave generated by a 5° wedge placed at the nozzle exit was also estimated, and the pressure profile was measured (Head et al. 2023).

A Ludwieg tube–type setup operates at Cambridge University (Baumgärtner et al. 2020). The test section is used to perform measurements in a miniaturized annular cascade. The first study focused on air, CO_2, R134a, and argon as working fluids in ideal gas states, and the objective was the assessment of the influence of specific heat ratio on the fluid dynamic losses in the annular cascade. Wall static pressure measurements were compared with simulations.

Learning from the experience gained with the FAST setup, TU Delft researchers recently designed the much smaller and simpler asymmetric shock tube for experiments on rarefaction waves (Chandrasekaran 2023). The triggering mechanism is a glass diaphragm. Preliminary experiments using D_6 at thermodynamic conditions for which nonclassical effects are theoretically predicted show that the speed of the wave, also measured in this case with a time-of-flight method, remained constant or slightly increased. More experiments are underway.

Derived measurement: property calculated with thermodynamic models starting from measured values; equilibrium can be assumed: the molecule vibrational relaxation time is very short due to the high collision frequency and fluid density

3.3.2. Measurement techniques. The velocity vector, pressure, temperature, possibly density, and—in supersonic flows—Mach number can be measured directly. From them, derived measurements can be obtained. Often challenges arise due to the high temperature of the fluid and/or the risk of condensation. For P measurements the materials of sensors and lines must be chemically compatible with the fluid and suitable for relatively high temperatures; in addition, transducers are often sensitive to temperature and thus require combined P, T calibration. In case of remotely mounted sensors, condensation may occur within lines, implying errors due to liquid head and menisci formation. Moreover, the frequency response much decreases due to the very low vapor mass flow rate feeding the line. These issues can be solved by periodically flushing the lines (Head 2021, Conti et al. 2022a). If the flow is subsonic, the total pressure can be measured directly with a pressure probe, while for supersonic flows additional data are needed to solve the jump relation across the probe-induced bowed shock (Manfredi et al. 2023). In the case of air in ideal gas states, P_t upstream of the probe-head shock is retrieved via probe calibration, usually unavailable for nonideal flows because a fluid- and condition-specific calibration would be required, being P_t losses depend on Z and Γ. Probes must be carefully designed because they are subjected to high mechanical loads and vibrations caused by the high density and speed of the fluid.

Velocity measurements can be obtained by means of directional (multi-hole) pressure probes, hot wire anemometry, and—if the fluid is transparent—LDV or particle image velocimetry (PIV). The successful use of directional multi-hole probes in NICFD flows is not documented in the literature yet, and first attempts resulted in quite inaccurate measurements (see Schaffer et al. 2022). Two-dimensional LDV has been recently employed to measure the flow velocity of MM vapor (Gallarini et al. 2021) by solving the challenge of seeding such a high-temperature flow. The seeding method is also applicable to PIV. Hot wire anemometry is suitable to measure the velocity field. Its high-frequency response may allow resolution of turbulence fluctuations. However, the need for wire robustness limits miniaturization and hence time resolution. Preliminary work is documented by Hake et al. (2022).

Flow temperature can be measured with thermocouple or resistance thermometers. The total temperature measurement in high-speed flows requires calibration to retrieve the recovery factor r, which depends on the fluid, the Mach number, and the operating conditions. Calibration supported by CFD simulations is considered reliable due to the simple geometry of the sensing element and its limited impact on the r value.

Density gradients in transparent vapor flows can be visualized by means of schlieren techniques. In NICFD flows, sensitivity to density gradients is higher than in ideal gas flows due to the higher density. For a given density ratio gradient, the light deviation is proportional to the total flow density and to the Gladstone-Dale constant K (Conti et al. 2017). Background-oriented schlieren techniques can also measure density gradients (Sundermeier et al. 2023). Density values can be obtained by integration if a reference value can be measured. Spatial resolution may be limited by both background pattern dimension and camera resolution. Distortions induced by high-density gradients may result in blurred patterns. For high-temperature flows, density variation along the optical path due to the natural convection of surrounding air may cause further errors.

4. APPLICATIONS

4.1. Fluid Machines

NICFD effects can be relevant in supersonic and transonic turboexpanders/compressors and may be appreciable even if the flow Mach number is lower, such as, e.g., in turbopumps operating in the compressible liquid regime.

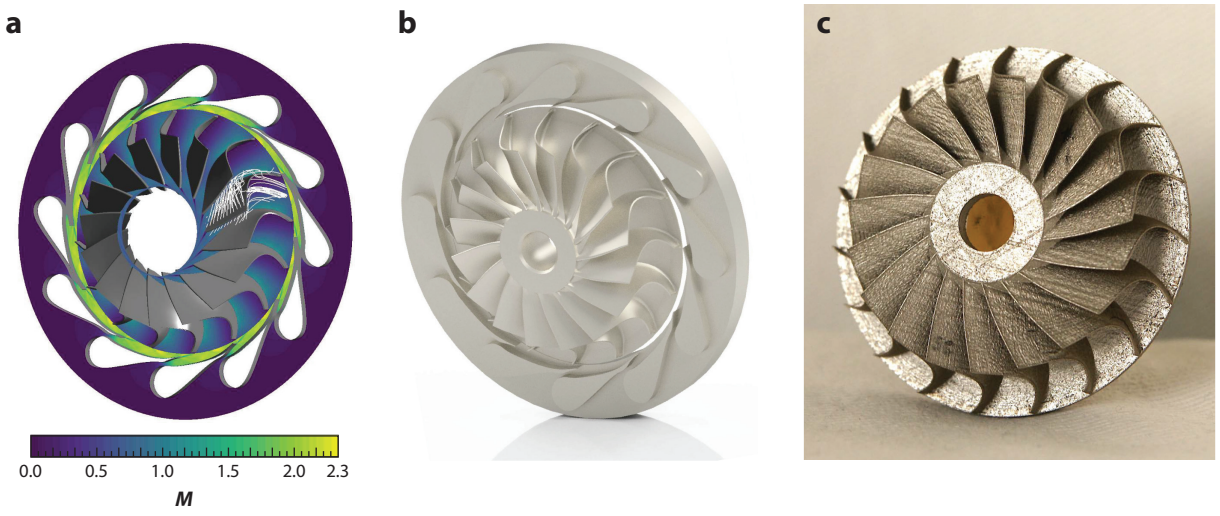

Figure 7

The high-speed (≈100 krpm) supersonic ORC turbine being realized for the ORCHID (**Figure 6*c***). The working fluid is MM. (*a*) Contour plot of *M* at mid-span (RANS simulation with a stator/rotor mixing-plane interface). (*b*) Computer-aided design rendering of the geometry designed by means of CFD and mechanical considerations. (*c*) Three-dimensional printing of the stainless steel rotor. Abbreviations: CFD, computational fluid dynamics; *M*, Mach number; MM, hexamethyldisiloxane; ORC, organic Rankine cycle; ORCHID, organic Rankine cycle hybrid integrated device; RANS, Reynolds-averaged Navier-Stokes.

The stator vanes of turbines of ORC power plants often operate in the NICFD regime (Macchi 1977, Colonna et al. 2015). **Figure 7** shows an exemplary high-speed ORC turbine suitable for waste heat recovery from propulsion engines. Working fluids of ORC power plants are usually HMC fluids. Currently, BZT fluids are not employed; however, they may be suitable for highly miniaturized ORC systems. Although nonideal gas dynamic effects (Section 2.2) may occur in ORC nozzle cascades for particular operating conditions (Romei et al. 2020), these conditions have never been realized in actual machines.

Compressors of supercritical CO_2 (sCO_2) power plants (Angelino 1968) operate with the fluid in highly nonideal states. The working fluid at the compressor inlet is in states close to the vapor-liquid critical point as this reduces the needed power, and in these conditions the flow is highly nonideal and compressible.

According to nondimensional analysis, the volume ratio V_R, the size parameter *SP*, the compressibility factor *Z*, and the isentropic pressure-volume exponent γ_{Pv} (or Γ) are the parameters characterizing the design and fluid dynamic performance of turbomachinery operating with the working fluid in nonideal thermodynamic states (even partially) along the process. Durá Galiana et al. (2016) and Giuffré & Pini (2020) found that, if NICFD effects are relevant, mixing losses (i.e., trailing-edge and shock losses) are largely affected by the local γ_{Pv} value, which in turn is influenced by the local value of *Z*. This is also due to the different patterns and strengths of fans, shocks, wakes, and secondary flows. Therefore, any engineering loss model must account for the effect of γ_{Pv}, especially on these loss sources. The influence of thermodynamic nonideality of the fluid can also affect machine operability. For example, the stall margin can be enhanced in radial compressors (Lettieri et al. 2014), and critical choking can occur in turbines (Tosto et al. 2022).

Volume ratio: $V_R = \frac{\dot{V}_{out}}{\dot{V}_{in}} = \frac{\rho_{in}}{\rho_{out}}$, where $\dot{V}_{in}, \dot{V}_{out}$ are the volumetric flow rate at the inlet and outlet of the turbine (and vice versa for a compressor)

Size parameter: $SP = \sqrt{\dot{V}}/\Delta h_{is}^{0.25}$, where Δh_{is} is the isentropic enthalpy drop across the stage; *SP* has the dimensions of a length and is related to the dimension of a machine stage

Isentropic pressure-volume exponent: $\gamma_{Pv} = -\frac{v}{P}\frac{\partial P}{\partial v}_s$ is the exponent that generalizes the isentropic ideal gas relation $Pv^\gamma = \text{const.}$ for nonideal thermodynamic states

4.2. Heat Exchangers

Nonideal thermodynamic property effects play an important role in heat transfer if the fluid is at supercritical pressure, while, for dense vapors, heat transfer is qualitatively the same as for ideal

gases. Examples of heat exchangers operating at supercritical pressure are coolers, heaters, and regenerators of sCO_2 power plants, condensers of supercritical heat pumps, and heaters of supercritical ORC turbogenerators. At supercritical pressure, forced convection mechanisms are primarily influenced by the large gradients of thermophysical properties occurring in the proximity of the Widom line, where the peak value of heat capacity and the decrease in density, dynamic viscosity, and thermal conductivity moving from liquid- to gas-like states are considerable. The variation of the Prandtl number is appreciable, culminating at the pseudocritical state. The strong density variation leads to significant streamwise flow acceleration in the frequent case of constant area ducts. The density change may lead to significant buoyancy effects, which can trigger mixed convection. Heat transfer can therefore be enhanced or deteriorated, and the flow can become unstable and pulsating. Parameters that most affect convective heat transfer coefficients are the heat flux-to-flow rate ratio, the heat flux direction (heating/cooling), the flow direction (horizontal, vertical upward/downward), the cross-sectional channel shape, and the hydraulic diameter; see Yoo (2013) and Van Nieuwenhuyse et al. (2023), which also documents empirical correlations for supercritical pressure flows. These models express the Nusselt number as a function of the bulk Reynolds and Prandtl numbers, the wall-to-bulk density ratio, the average-to-bulk c_P ratio, and the Grashof number. These relations are calibrated for specific fluids (water, CO_2, and some refrigerants), flow directions, channel geometry, and operating conditions, while generally applicable models are still missing. The prediction of friction losses is usually based on correlations developed for subcritical pressure flows, corrected for the effect of thermophysical properties variation (Yoo 2013, Van Nieuwenhuyse et al. 2023).

4.3. Supercritical Fluid Injectors for Combustors

Critical processes in combustors of energy conversion systems (e.g., gas turbines, diesel and rocket engines) are fuel injection and mixing. The increase in combustor pressure is the unchanged trend since they were introduced because it entails better efficiency and reduced emissions. For an extensive treatment of supercritical injection, see the works of Bellan (2020) and Jofre & Urzay (2021). At such high pressures and temperatures, the thermodynamic conditions of the fuel (and possibly of the oxidizer) are supercritical; therefore, nonideal thermodynamic property effects have a relevant influence on the mixing process (see Section 2.4), which results in enhanced mixing and diffusion, thus producing a thicker flame front that reduces NO_x formation. Fuel-oxidizer mixing occurs in the free jet zone at the nozzle outlet, to a large extent downstream of the Mach disk that typically establishes. Thus, the prediction of flow structures and of the Mach disk location and size is pivotal to assess the mixing process, which is influenced by nonideal effects upstream of the Mach disk. Flow mixing can be accurately modeled via CFD (Müller et al. 2016). For example, Traxinger & Pfitzner (2021) simulated the injection of supercritical normal-hexane (C_6H_{14}) in quiescent nitrogen at subcritical dilute conditions. CFD simulations were satisfactorily compared with experimental data by Baab et al. (2016) and Förster et al. (2018). These studies show that the low pressure of the expanded jet is raised to the chamber pressure level by the strong disk shock; thus, downstream of the shock, the mixing occurs almost isobarically and in dilute gas conditions. However, nonideal thermodynamic effects ahead of the disk shock are so intense that they must be accurately modeled to obtain, for instance, the correct temperature profile of the mixing region.

SUMMARY POINTS

1. Research outcomes of the last two decades have been consolidated into a unitary framework, together with suitable terminology.

2. The differences between nonideal thermodynamic effects, nonideal gas dynamic effects, and the role of molecular complexity have been clarified.
3. Turbulence and heat transfer models applicable to ideal gas flows are also suitable for nonideal compressible fluid dynamic (NICFD) flows. Compressibility corrections to turbulence models have a negligible effect on the integral quantities. NICFD flows are less prone to instabilities except for flows evolving in the thermodynamic region of the Widom line.
4. Numerical methods for simulations of NICFD flows are well established. The first results of higher-order simulations, automated turbomachinery shape optimization, and uncertainty quantification methods are being documented.
5. Cubic equation of state models are almost always sufficiently accurate, except for nonclassical gas dynamics studies. Transport property models of fluids in nonideal states are inaccurate; however, normally this is uninfluential on flow simulation results.
6. Experiments and measurement techniques are challenging because of the unconventional working fluids and demanding operating conditions. Momentous experimental work has only recently started. Initial results are satisfactory.
7. The performance of machinery and devices benefits from the recent introduction of more accurate models and design methods that are bringing these components to the technological level of those operating with ideal gas flows.

FUTURE ISSUES

1. The experimental verification of most nonideal gas dynamic effects is still lacking and activities are underway. Turbulence physics and turbulent heat transfer in canonical flows should also be characterized experimentally.
2. Theory on the dissipation within boundary layers of nonideal flows in the presence of pressure gradients, heat transfer, and rotational effects is still limited or absent. Knowledge on instabilities in supercritical and dense vapor flows would benefit from further direct numerical simulations.
3. Better mixture thermophysical property models are needed and are under development. Computationally faster models and methods (e.g., equations of state in terms of energy and specific volume or data-driven models) should be further developed.
4. The development of directional pressure probes demands robust numerical calibration methods. The use of particle image velocimetry is within reach. Raman spectroscopy and Rayleigh scattering methods for measuring flow temperature and density warrant in-depth studies to assess their suitability.
5. It is desirable that the NICFD community foster current policies of open-science and open-source software. More reference data concerning numerical simulations, experiments, and software should be openly released in a structured manner.

DISCLOSURE STATEMENT

The authors are not aware of any biases that might be perceived as affecting the objectivity of this review.

ACKNOWLEDGMENTS

Ian Bell, Alexis Bohlin, Carlo De Servi, Bertrand Mercier, René Pecnik, Giacomo Persico, Luigi Quartapelle, Luca Sciacovelli, Teus van der Stelt, Luigi Vigevano, and Davide Vimercati contributed interesting discussions. Paolo Gajoni, Francesco Tosto, and Marta Zocca supported the generation of some figures and data.

This work is dedicated to the late Professor Alfred Kluwick.

LITERATURE CITED

Anders JB, Anderson WK, Murthy AV. 1999. Transonic similarity theory applied to a supercritical airfoil in heavy gases. *J. Aircraft* 36(6):957–64

Angelino G. 1968. Carbon dioxide condensation cycles for power production. *J. Eng. Power* 90:287–95

Baab S, Förster FJ, Lamanna G, Weigand B. 2016. Speed of sound measurements and mixing characterization of underexpanded fuel jets with supercritical reservoir condition using laser-induced thermal acoustics. *Exp. Fluids* 57(11):17213

Banuti DT. 2015. Crossing the Widom line—supercritical pseudo-boiling. *J. Supercrit. Fluids* 98:12–16

Bates JW, Montgomery DC. 1999. Some numerical studies of exotic shock wave behavior. *Phys. Fluids* 11(2):462–75

Baumgärtner D, Otter JJ, Wheeler APS. 2020. The effect of isentropic exponent on transonic turbine performance. *J. Turbomach.* 142(8):08100710

Bell IH, Alpert BK. 2021. Efficient and precise representation of pure fluid phase equilibria with Chebyshev expansions. *Int. J. Thermophys.* 42:7516

Bell IH, Laesecke A. 2016. *Viscosity of refrigerants and other working fluids from residual entropy scaling*. Paper presented at the 16th International Refrigeration and Air Conditioning Conference at Purdue University, West Lafayette, IN, July 11–14

Bellan J, ed. 2020. *High-Pressure Flows for Propulsion Applications*. Reston, VA: AIAA

Beltrame F, De Servi C, Head AJ, Pini M, Schrijer F, Colonna P. 2021. First experiments and commissioning of the ORCHID nozzle test section. In *Proceedings of the 3rd International Seminar on Non-Ideal Compressible Fluid Dynamics for Propulsion and Power*, ed. M Pini, C De Servi, A Spinelli, F di Mare, A Guardone, pp. 169–78. Cham, Switz.: Springer

Bethe HA. 1942. *The theory of shock waves for an arbitrary equation of state*. Tech. Rep. 545, Off. Sci. Res. Dev., New York

Bier K, Ehrler F, Niekrawietz M. 1990. Experimental investigation and computer analysis of spontaneous condensation in stationary nozzle flow of CO_2-air mixtures. In *Adiabatic Waves in Liquid-Vapor Systems*, ed. GEA Meier, PA Thompson, pp. 113–27. Berlin: Springer

Bradshaw P. 1977. Compressible turbulent shear layers. *Annu. Rev. Fluid Mech.* 9:33–52

Callen HB. 1985. *Thermodynamics and an Introduction to Thermostatistics*. Toronto: Wiley. 2nd ed.

Cammi G, Spinelli A, Cozzi F, Guardone A. 2021. Automatic detection of oblique shocks and simple waves in schlieren images of two-dimensional supersonic steady flows. *Measurement* 168:10826014

Castier M, Cabral VF. 2012. Pure saturated gases with predicted negative fundamental derivative of gas dynamics. *Fluid Phase Equilib.* 334:128–36

Chandrasekar D, Prasad P. 1991. Transonic flow of a fluid with positive and negative nonlinearity through a nozzle. *Phys. Fluids A* 3(3):427–38

Chandrasekaran NB. 2023. *Nonclassical gasdynamics: theory and experiments on nonlinear wave propagation in BZT fluids*. PhD Thesis, Delft Univ. Technol., Delft, Neth.

Chichester JC, Huber ML. 2008. *Documentation and assessment of the transport property model for mixtures implemented in NIST REFPROP* (version 8.0). Tech. Rep. NISTIR 6650, Natl. Inst. Stand. Technol., Boulder, CO

Cinnella P. 2006. Roe-type schemes for dense gas flow computations. *Comput. Fluids* 35(10):1264–81

Cinnella P, Hercus SJ. 2010. Robust optimization of dense gas flows under uncertain operating conditions. *Comput. Fluids* 39(10):1893–908

Colonna P, Casati E, Trapp C, Mathijssen T, Larjola J, et al. 2015. Organic Rankine cycle power systems: from the concept to current technology, applications, and an outlook to the future. *J. Eng. Gas Turb. Power* 137(10):10080119

Colonna P, Guardone A. 2006. Molecular interpretation of nonclassical gas dynamics of dense vapors under the van der Waals model. *Phys. Fluids* 18(5):05610114

Colonna P, Guardone A, Nannan NR, van der Stelt TP. 2009. On the computation of the fundamental derivative of gas dynamics using equations of state. *Fluid Phase Equilib.* 286(1):43–54

Colonna P, Rebay S. 2004. Numerical simulation of dense gas flows on unstructured grids with an implicit high resolution upwind Euler solver. *Int. J. Numer. Meth. Fluids* 46(7):735–65

Colonna P, Silva P. 2003. Dense gas thermodynamic properties of single and multi-component fluids for fluid dynamics simulations. *J. Fluids Eng.* 125(3):414–27

Conti CC, Fusetti A, Spinelli A, Gaetani P, Guardone A. 2022a. Pneumatic system for pressure probe measurements in transient flows of non-ideal vapors subject to line condensation. *Measurement* 192:11080213

Conti CC, Fusetti A, Spinelli A, Guardone A. 2022b. Shock loss measurements in non-ideal supersonic flows of organic vapors. *Exp. Fluids* 63(7):11711

Conti CC, Spinelli A, Cammi G, Zocca M, Cozzi F, Guardone A. 2017. *Schlieren visualizations of non-ideal compressible fluid flows*. Paper presented at the 13th International Conference on Heat Transfer, Fluid Mechanics and Thermodynamics, Portoroz, Slovenia, July 17–19

Conti CC, Spinelli A, Guardone A. 2021. Similarity parameters for non-ideal one-dimensional isentropic expansions. In *Proceedings of the 3rd International Seminar on Non-Ideal Compressible Fluid Dynamics for Propulsion and Power*, ed. M Pini, C De Servi, A Spinelli, F di Mare, A Guardone, pp. 26–35. Cham, Switz.: Springer

Cramer MS, Best LM. 1991. Steady, isentropic flows of dense gases. *Phys. Fluids A* 3(4):219–26

Cramer MS, Fry NR. 1993. Nozzle flows of dense gases. *Phys. Fluids A* 5(5):1246–59

Cramer MS, Park SH, Watson LT. 1997. Numerical verification of scaling laws for shock-boundary layer interactions in arbitrary gases. *J. Fluids Eng.* 119(1):67–73

Cramer MS, Whitlock ST, Tarkenton GM. 1996. Transonic and boundary layer similarity laws in dense gases. *J. Fluids Eng.* 118(3):481–85

Dettleff G, Thompson PA, Meier EA, Speckmann H. 1979. An experimental study of liquefaction shock waves. *J. Fluid Mech.* 95:279–304

Duan L, Zheng Q, Jiang Z, Wang J. 2021. Dense gas effect on small-scale structures of compressible isotropic turbulence. *Phys. Fluids* 33(11):11511323

Duff K. 1966. *Non-equilibrium condensation of carbon dioxide in supersonic nozzles*. PhD Thesis, Mass. Inst. Technol., Cambridge, Mass.

Durá Galiana FJ, Wheeler APS, Ong J. 2016. A study of trailing-edge losses in organic Rankine cycle turbines. *J. Turbomach.* 138(12):1210039

Fergason SH, Guardone A, Argrow BM. 2003. Construction and validation of a dense gas shock tube. *J. Thermophys. Heat Transf.* 17(3):326–33

Förster FJ, Baab S, Steinhausen C, Lamanna G, Ewart P, Weigand B. 2018. Mixing characterization of highly underexpanded fluid jets with real gas expansion. *Exp. Fluids* 59(3):44

Gallarini S, Cozzi F, Spinelli A, Guardone A. 2021. Direct velocity measurements in high-temperature non-ideal vapor flows. *Exp. Fluids* 62(10):19918

Giauque A, Corre C, Vadrot A. 2020. Direct numerical simulations of forced homogeneous isotropic turbulence in a dense gas. *J. Turbul.* 21(3):186–208

Giuffré A, Pini M. 2020. Design guidelines for axial turbines operating with non-ideal compressible flows. *J. Eng. Gas Turb. Power* 143(1):011004

Gloerfelt X, Robinet JC, Sciacovelli L, Cinnella P, Grasso F. 2020. Dense-gas effects on compressible boundary-layer stability. *J. Fluid Mech.* 893:A1941

Gori G, Zocca M, Cammi G, Spinelli A, Congedo PM, Guardone A. 2020a. Accuracy assessment of the non-ideal computational fluid dynamics model for siloxane MDM from the open-source SU2 suite. *Eur. J. Mech. B/Fluids* 79:109–20

Gori G, Zocca M, Guardone A, Le Maître OP, Congedo PM. 2020b. Bayesian inference of thermodynamic models from vapor flow experiments. *Comput. Fluids* 205:10455017

Gross J, Sadowski G. 2001. Perturbed-chain SAFT: an equation of state based on a perturbation theory for chain molecules. *Ind. Eng. Chem. Res.* 40(4):1244–60

Guardone A, Colonna P, Casati E, Rinaldi E. 2014. Nonclassical gasdynamics of BZT mixtures. *J. Fluid Mech.* 741:681–701

Guardone A, Vigevano L. 2002. Roe linearization for the van der Waals gas. *J. Comput. Phys.* 175(1):50–78

Guardone A, Vimercati D. 2016. Exact solutions to non-classical steady nozzle flows of Bethe-Zel'dovich-Thompson fluids. *J. Fluid Mech.* 800:278–306

Hake L, Sundermeier S, Cakievski L, Bäumer J, aus der Wiesche S, et al. 2022. *Hot-wire anemometry in high subsonic organic vapor flows*. Paper presented at ASME Turbo Expo 2022: Turbomachinery Technical Conference and Exposition, Rotterdam, Neth., June 13–17

Head AJ. 2021. *Novel experiments for the investigation of non-ideal compressible fluid dynamics*. PhD Thesis, Delft Univ. Technol., Delft, Neth.

Head AJ, Michelis T, Beltrame F, Fuentes Monjas B, Casati E, et al. 2023. Mach number estimation and pressure profile measurements of expanding dense organic vapors. In *Proceedings of the 4th International Seminar on Non-Ideal Compressible Fluid Dynamics for Propulsion and Power*, ed. M White, T El Samad, I Karathanassis, A Sayma, M Pini, A Guardone, pp. 229–38. Cham, Switz.: Springer

Jofre L, Urzay J. 2021. Transcritical diffuse-interface hydrodynamics of propellants in high-pressure combustors of chemical propulsion systems. *Prog. Energy Combust. Sci.* 82:100877

Kawai S. 2019. Heated transcritical and unheated non-transcritical turbulent boundary layers at supercritical pressures. *J. Fluid Mech.* 865:563–601

Kluwick A. 1993. Transonic nozzle flow of dense gases. *J. Fluid Mech.* 247:661–88

Kluwick A. 1994. Interacting laminar boundary layers of dense gases. In *Fluid- and Gasdynamics. Acta Mechanica*, ed. GH Schnerr, R Bohning, W Frank, K Bühler, pp. 335–49. Vienna: Springer

Kluwick A. 2001. Rarefaction shocks. In *Handbook of Shock Waves*, ed. G Ben-Dor, O Igra, T Elperin, pp. 339–411. San Diego, CA: Academic

Kluwick A. 2004. Internal flows of dense gases. *Acta Mech.* 169:123–43

Kutateladze SS, Nakoryakov VE, Borisov AA. 1987. Rarefaction waves in liquid and gas-liquid media. *Annu. Rev. Fluid Mech.* 19:577–600

Lettieri C, Baltadjiev N, Casey M, Spakovszky Z. 2014. Low-flow-coefficient centrifugal compressor design for supercritical CO_2. *J. Turbomach.* 136(8):0810089

Lettieri C, Yang D, Spakovszky Z. 2015. An investigation of condensation effects in supercritical carbon dioxide compressors. *J. Eng. Gas Turb. Power* 137(8):0826028

Liu TP. 1976. The entropy condition and the admissibility of shocks. *J. Math. Anal. Appl.* 53(1):78–88

Lopez-Echeverry JS, Reif-Acherman S, Araujo-Lopez E. 2017. Peng-Robinson equation of state: 40 years through cubics. *Fluid Phase Equilib.* 447:39–71

Lötgering-Lin O, Gross J. 2015. Group contribution method for viscosities based on entropy scaling using the perturbed-chain polar statistical associating fluid theory. *Ind. Eng. Chem. Res.* 54(32):7942–52

Ly N, Ihme M. 2022. Destabilization of binary mixing layer in supercritical conditions. *J. Fluid Mech.* 945:R2

Ly N, Rusak Z, Wang S. 2018. Swirling flow states of compressible single-phase supercritical fluids in a rotating finite-length straight circular pipe. *J. Fluid Mech.* 849:576–614

Macchi E. 1977. Design criteria for turbines operating with fluids having a low speed of sound. In *Lecture Series 100 on Closed-Cycle Gas Turbines*. Rhode-Saint-Genése, Belg.: Von Karman Inst. Fluid Dyn.

Manfredi M, Persico G, Spinelli A, Gaetani P, Dossena V. 2023. Design and commissioning of experiments for supersonic ORC nozzles in linear cascade configuration. *Appl. Therm. Eng.* 224:11999611

Mathijssen T, Gallo M, Casati E, Nannan NR, Zamfirescu C, et al. 2015. The flexible asymmetric shock tube (FAST)—Ludwieg tube facility for wave propagation measurements in high-temperature vapours of organic fluids. *Exp. Fluids* 56(10):19512

McQuarrie DA. 1976. *Statistical Mechanics*. New York: Harper Collins

Menikoff R, Plohr BJ. 1989. The Riemann problem for fluid flow of real materials. *Rev. Mod. Phys.* 61(1):75–130

Mercier B, Chandrasekaran NB, Colonna P. 2023. Speed of sound measurements in dense siloxane D_6 vapour at temperatures up to 645 K by means of a new prismatic resonator. *J. Chem. Eng. Data* 68(3):561–73

Milan PJ, Hickey JP, Wang X, Yang V. 2021. Deep-learning accelerated calculation of real-fluid properties in numerical simulation of complex flowfields. *J. Comput. Phys.* 444:11056725

Müller H, Niedermeier CA, Matheis J, Pfitzner M, Hickel S. 2016. Large-eddy simulation of nitrogen injection at trans- and supercritical conditions. *Phys. Fluids* 28(1):01510228

Nannan NR, Guardone A, Colonna P. 2013. On the fundamental derivative of gas dynamics in the vapor-liquid critical region of single-component typical fluids. *Fluid Phase Equilib.* 337:259–73

Nannan RN, Guardone A, Colonna P. 2014. Critical point anomalies include expansion shock waves. *Phys. Fluids* 26(2):021701

Novak LT. 2011. Fluid viscosity-residual entropy correlation. *Int. J. Chem. React. Eng.* 9(1):A107

Otero GJ, Patel A, Diez R, Pecnik R. 2018. Turbulence modelling for flows with strong variations in thermophysical properties. *Int. J. Heat Fluid Flow* 73:114–23

Pecnik R, Patel A. 2017. Scaling and modelling of turbulence in variable property channel flows. *J. Fluid Mech.* 823:R1–12

Peeters JWR, Pecnik R, Rohde M, van der Hagen THJJ, Boersma BJ. 2016. Turbulence attenuation in simultaneously heated and cooled annular flows at supercritical pressure. *J. Fluid Mech.* 799:505–40

Persico G, Rodriguez-Fernandez P, Romei A. 2019. High-fidelity shape optimization of non-conventional turbomachinery by surrogate evolutionary strategies. *J. Turbomach.* 141(8):08101011

Pini M, De Servi C. 2020. Entropy generation in laminar boundary layers of non-ideal fluid flows. In *Proceedings of the 4th International Seminar on Non-Ideal Compressible Fluid Dynamics for Propulsion and Power*, ed. F di Mare, A Spinelli, M Pini, pp. 104–17. Cham, Switz.: Springer

Pini M, Spinelli A, Persico G, Rebay S. 2015. Consistent look-up table interpolation method for real-gas flow simulations. *Comput. Fluids* 107:178–88

Poling BE, Prausnitz JM, O'Connell JP. 2001. *Properties of Gases and Liquids*. New York: McGraw-Hill. 5th ed.

Qi J, Xu J, Han K, Jahn I. 2022. Development and validation of a Riemann solver in OpenFOAM for non-ideal compressible fluid dynamics. *Eng. Appl. Comp. Fluid* 16:116–40

Quiñones-Cisneros SE, Pollak S, Schmidt KAG. 2021. Friction theory model for thermal conductivity. *J. Chem. Eng. Data* 66(11):4215–27

Quiñones-Cisneros SE, Zéberg-Mikkelsen CK, Stenby EH. 2000. The friction theory (*f-theory*) for viscosity modeling. *Fluid Phase Equilib.* 169(2):249–76

Razaaly N, Persico G, Congedo PM. 2019. Impact of geometric, operational, and model uncertainties on the non-ideal flow through a supersonic ORC turbine cascade. *Energy* 169:213–27

Re B, Abgrall R. 2022. A pressure-based method for weakly compressible two-phase flows under a Baer-Nunziato type model with generic equations of state and pressure and velocity disequilibrium. *Int. J. Numer. Meth. Fluids* 94(8):1183–232

Reinker F, Wagner R, Hake L, aus der Wiesche S. 2021. High subsonic flow of an organic vapor past a circular cylinder. *Exp. Fluids* 62(3):5416

Ren J, Fu S, Pecnik R. 2019a. Linear instability of Poiseuille flows with highly non-ideal fluids. *J. Fluid Mech.* 859:89–125

Ren J, Marxen O, Pecnik R. 2019b. Boundary-layer stability of supercritical fluids in the vicinity of the Widom line. *J. Fluid Mech.* 871:831–64

Reynolds WC, Colonna P. 2018. *Thermodynamics: Fundamentals and Engineering Applications*. Cambridge, UK: Cambridge Univ. Press

Rinaldi E, Colonna P, Pecnik R. 2015. Flux-conserving treatment of non-conformal interfaces for finite-volume discretization of conservation laws. *Comput. Fluids* 120:126–39

Romei A, Vimercati D, Persico G, Guardone A. 2020. Non-ideal compressible flows in supersonic turbine cascades. *J. Fluid Mech.* 882:A1226

Rubino A, Colonna P, Pini M. 2021. Adjoint-based unsteady optimization of turbomachinery operating with nonideal compressible flows. *J. Propul. Power* 37(6):910–18

Rubino A, Pini M, Kosec M, Vitale S, Colonna P. 2018. A look-up table method based on unstructured grids and its application to non-ideal compressible fluid dynamic simulations. *J. Comput. Sci.* 28:70–77

Schaffer C, Speck K, Gummer V. 2022. Numerical calibration and investigation of the influence of Reynolds number on measurements with five-hole probes in compressible flows. *J. Turbomach.* 144(9):091010

Schuster D, Ince Y, Giauque A, Corre C. 2023. Assessment of compressibility corrections for RANS simulations of real gas flows using SU2. In *Proceedings of the 4th International Seminar on Non-Ideal Compressible Fluid Dynamics for Propulsion and Power*, ed. M White, T El Samad, I Karathanassis, A Sayma, M Pini, A Guardone, pp. 82–90. Cham, Switz.: Springer

Sciacovelli L, Cinnella P, Gloerfelt X. 2018. A priori tests of RANS models for turbulent channel flows of a dense gas. *Flow Turbul. Combust.* 101(2):295–315

Sciacovelli L, Cinnella P, Grasso F. 2017. Small-scale dynamics of dense gas compressible homogeneous isotropic turbulence. *J. Fluid Mech.* 825:515–49

Sciacovelli L, Gloerfelt X, Passiatore D, Cinnella P, Grasso F. 2020. Numerical investigation of high-speed turbulent boundary layers of dense gases. *Flow Turbul. Combust.* 105(2):555–79

Sharan N, Bellan J. 2021. Investigation of high-pressure turbulent jets using direct numerical simulation. *J. Fluid Mech.* 922:A2448

Span R. 2000. *Multiparameter Equations of State*. Berlin: Springer-Verlag

Spinelli A, Cammi G, Gallarini S, Zocca M, Cozzi F, et al. 2018. Experimental evidence of non-ideal compressible effects in expanding flow of a high molecular complexity vapor. *Exp. Fluids* 59(8):12616

Spinelli A, Guardone A, Cozzi F, Carmine M, Cheli R, et al. 2017. Experimental observation of non-ideal nozzle flow of siloxane vapor MDM. *Energy Procedia* 129:1125–32

Sundermeier SC, Matar C, Aus der Wiesche S, Cinnella P, Hake L, Gloerfelt X. 2023. Experimental and numerical study of transonic flow of an organic vapor past a circular cylinder. In *Proceedings of the 4th International Seminar on Non-Ideal Compressible Fluid Dynamics for Propulsion and Power*, ed. M White, T El Samad, I Karathanassis, A Sayma, M Pini, A Guardone, pp. 209–16. Cham, Switz.: Springer

Swesty FD. 1996. Thermodynamically consistent interpolation for equation of state tables. *J. Comput. Phys.* 127(1):118–27

Thompson PA. 1971. A fundamental derivative in gasdynamics. *Phys. Fluids* 14(9):1843–49

Thompson PA, Lambrakis KC. 1973. Negative shock waves. *J. Fluid Mech.* 60:187–208

Tosto F. 2023. *Modeling and characterization of nonideal compressible flows in unconventional turbines*. PhD Thesis, Delft Univ. Technol., Delft, Neth.

Tosto F, Giuffré A, Colonna P, Pini M. 2022. Flow deviation and critical choking in transonic turbine cascades operating with non-ideal compressible flows. *J. Glob. Propul. Power Soc.* 6:181–99

Touber E. 2019. Small-scale two-dimensional turbulence shaped by bulk viscosity. *J. Fluid Mech.* 875:974–1003

Traxinger C, Pfitzner M. 2021. Effect of nonideal fluid behavior on the jet mixing process under high-pressure and supersonic flow conditions. *J. Supercrit. Fluids* 172:10519517

Trettel A, Larsson J. 2016. Mean velocity scaling for compressible wall turbulence with heat transfer. *Phys. Fluids* 28(2):026102

Vadrot A, Giauque A, Corre C. 2021. Direct numerical simulations of temporal compressible mixing layers in a Bethe–Zel'dovich–Thompson dense gas: influence of the convective Mach number. *J. Fluid Mech.* 922:A536

Van Nieuwenhuyse J, Lecompte S, De Paepe M. 2023. Current status of the thermohydraulic behavior of supercritical refrigerants: a review. *Appl. Therm. Eng.* 218:11920120

Vimercati D, Gori G, Guardone A. 2018a. Non-ideal oblique shock waves. *J. Fluid Mech.* 847:266–85

Vimercati D, Guardone A. 2018. On the numerical simulation of non-classical quasi-1D steady nozzle flows: capturing sonic shocks. *Appl. Math. Comput.* 319:617–32

Vimercati D, Kluwick A, Guardone A. 2018b. Oblique waves in steady supersonic flows of Bethe-Zel'dovich-Thompson fluids. *J. Fluid Mech.* 855:445–68

Vimercati D, Kluwick A, Guardone A. 2020. Shock interactions in two-dimensional steady flows of Bethe-Zel'dovich-Thompson fluids. *J. Fluid Mech.* 887:A1226

Vitale S, Albring TA, Pini M, Gauger NR, Colonna P. 2017. Fully turbulent discrete adjoint solver for non-ideal compressible flow applications. *J. Glob. Propul. Power Soc.* 1:252–70

Vitale S, Gori G, Pini M, Guardone A, Economon TD, et al. 2015. *Extension of the SU2 open source CFD code to the simulation of turbulent flows of fluids modelled with complex thermophysical laws*. Paper presented at 22nd AIAA Fluid Dynamics Conference, Dallas, AIAA Pap. 2015-2760

Vitale S, Pini M, Colonna P. 2020. Multi-stage turbomachinery design using the discrete adjoint method within the open-source software SU2. *J. Propul. Power* 36(3):465–78

Wheeler APS, Ong J. 2013. The role of dense gas dynamics on organic Rankine cycle turbine performance. *J. Eng. Gas Turb. Power* 135(10):1026039

Yang X, Xiao X, Thol M, Richter M, Bell IH. 2022. Linking viscosity to equations of state using residual entropy scaling theory. *Int. J. Thermophys.* 43(12):18324

Yoo JY. 2013. The turbulent flows of supercritical fluids with heat transfer. *Annu. Rev. Fluid Mech.* 45:495–525

Zamfirescu C, Guardone A, Colonna P. 2008. Admissibility region for rarefaction shock waves in dense gases. *J. Fluid Mech.* 599:363–81

Zel'dovich YB. 1946. On the possibility of rarefaction shock waves. *Zh. Eksp. Teor. Fiz.* 4:363–64

Zocca M. 2018. *Experimental Observation of Supersonic Non-Ideal Compressible-Fluid Flows*. PhD Thesis, Politecnico di Milano, Italy

Zocca M, Gajoni P, Guardone A. 2023. NIMOC: a design and analysis tool for supersonic nozzles under non-ideal compressible flow conditions. *J. Comput. Appl. Math.* 429:11521015

Zocca M, Guardone A, Cammi G, Cozzi F, Spinelli A. 2019. Experimental observation of oblique shock waves in steady non-ideal flows. *Exp. Fluids* 60(6):10112

Annual Review of Fluid Mechanics

Volume 56, 2024

Contents

Interfacial Dynamics Pioneer Stephen H. Davis (1939–2021)
Michael J. Miksis, G. Paul Neitzel, and Peter W. Voorhees 1

The Early Days and Rise of Turbulence Simulation
John Kim and Anthony Leonard 21

Flows Over Rotating Disks and Cones
P. Henrik Alfredsson, Kentaro Kato, and R.J. Lingwood 45

Turbulent Drag Reduction by Streamwise Traveling Waves of Wall-Normal Forcing
Koji Fukagata, Kaoru Iwamoto, and Yosuke Hasegawa 69

Gas Microfilms in Droplet Dynamics: When Do Drops Bounce?
James E. Sprittles 91

Fluid Dynamics of Squirmers and Ciliated Microorganisms
Takuji Ishikawa 119

Vortices and Forces in Biological Flight: Insects, Birds, and Bats
Hao Liu, Shizhao Wang, and Tianshu Liu 147

The Fluid Mechanics of Female Reproduction: A Review of the Biofluid Mechanics of Pregnancy and Delivery
Megan C. Leftwich and Alexa C. Baumer 171

Statistical Models for the Dynamics of Heavy Particles in Turbulence
J. Bec, K. Gustavsson, and B. Mehlig 189

Advances in Modeling Dense Granular Media
Ken Kamrin, Kimberly M. Hill, Daniel I. Goldman, and Jose E. Andrade 215

Nonideal Compressible Fluid Dynamics of Dense Vapors and Supercritical Fluids
Alberto Guardone, Piero Colonna, Matteo Pini, and Andrea Spinelli 241

The Dynamics of Jupiter's and Saturn's Weather Layers: A Synthesis After *Cassini* and *Juno*
Peter L. Read 271

Bubble Plumes in Nature
Silvana S.S. Cardoso and Julyan H.E. Cartwright 295

Deformation and Breakup of Bubbles and Drops in Turbulence
Rui Ni 319

Large-Scale Eddy-Mean Flow Interaction in the Earth's Extratropical Atmosphere
Noboru Nakamura 349

Gas–Particle Dynamics in High-Speed Flows
Jesse Capecelatro and Justin L. Wagner 379

Building Ventilation: The Consequences for Personal Exposure
Rajesh K. Bhagat, Stuart B. Dalziel, M.S. Davies Wykes, and P.F. Linden 405

Molecular Mechanics of Liquid and Gas Slip Flow
Nicolas G. Hadjiconstantinou 435

Multiscale Velocity Gradients in Turbulence
Perry L. Johnson and Michael Wilczek 463

Fluid-Elastic Interactions Near Contact at Low Reynolds Number
Bhargav Rallabandi 491

Learning Nonlinear Reduced Models from Data with Operator Inference
Boris Kramer, Benjamin Peherstorfer, and Karen E. Willcox 521

Flow Mechanics in Ablative Thermal Protection Systems
Nagi N. Mansour, Francesco Panerai, Jean Lachaud, and Thierry Magin 549

Fluid Dynamics of Airtanker Firefighting
Dominique Legendre 577

Indexes

Cumulative Index of Contributing Authors, Volumes 1–56 605

Cumulative Index of Article Titles, Volumes 1–56 617

Errata

An online log of corrections to *Annual Review of Fluid Mechanics* articles may be found at http://www.annualreviews.org/errata/fluid